Thesis/
Reports
Heimes,
F. J.

SPECTRAL VARIABILITY IN MOUNTAIN TERRAIN

F. J. Heimes and J. A. Smith

THESIS
AND
REPORTS
Heimes

SPECTRAL VARIABILITY IN MOUNTAIN TERRAIN

F.J. Heimes and J.A. Smith

Final Report
Rocky Mountain Forest and Range Experiment Station
U.S. Forest Service
Cooperative Agreement 16-625-CA

June, 1977

Department of Earth Resources
Colorado State University
Fort Collins, Colorado 80523

LIBRARY COPY
ROCKY MT. FOREST & RANGE
EXPERIMENT STATION

THE FINDINGS IN THIS REPORT ARE NOT TO BE CONSTRUED AS AN OFFICIAL USFS POSITION, UNLESS SO DESIGNATED BY OTHER AUTHORIZED DOCUMENTS.

LIBRARY COPY
ROCKY MT. FOREST & RANGE
EXPERIMENT STATION

ABSTRACT

Mixtures of scene components which fall within a resolution element affect the spectral response from that element. Heterogenous characteristics of natural scenes can result in large variations in proportions and types of scene components. This, can cause wide variability in spectral response between resolution elements making accurate classification of vegetation types difficult. A key to reducing problems caused by mixtures may lie in understanding effects of scene components on spectral response.

This study investigated relationships of primary scene components to spectral response in the visible and near infrared regions of the spectrum. Two high-elevation test sites near Leadville, Colorado were utilized, both in a lodgepole pine (Pinus contorta) community. One test site, M-3, consisted of a relatively simple scene with a wide range of component proportions, while the other site, IH-1, contained a more complex scene with less variation in component proportions. A tower tramway system was used to support data collection instruments above the forest canopy. The instrument used has the unique capability of providing a photographic record of the exact scene for which the spectral response is measured. Accompanying broad-band black and white photographs were used to estimate scene proportions. A predominant scene component that was present for both sites was shadowed areas. Shadows indirectly provide a measure of three dimensional structure and relative sun-angle effects on spectral response. Other primary scene components

included forest canopy and various understory constituents. Estimation of these proportions was accomplished by video density slicing each of the black and white photographic negatives. Estimated errors for this technique ranged from approximately 3-10%. A linear prediction model was used to estimate spectral irradiance from broad band irradiance. The mean percentage error from this method ranged from approximately 4 to 7%.

A simple linear regression model was used to relate primary scene components to scene spectral response. Eighty-three observations from the M-3 site and twenty-four observations from the IH-1 site were used in the analysis. Data were collected during August and September of 1976. Solar zenith angles ranged from 35-65^{o}. Regression results for data collected over the M-3 site resulted in R^2 values ranging from .86 to .99. R^2 values for equations developed from data for the more complex IH-1 site ranged from .46 to .88. The reduced effectiveness of the regression equations developed on IH-1 data appears to be a function of the larger errors in definition of primary scene components and subsequent estimation of their proportions.

Results from this study lend credibility to the theory of linear relationships between proportions of scene components and scene spectral response. Scene structure and orientation also must be considered, however, with respect to their effect on spectral response.

FORWARD

The research described in this report was supported under Cooperative Agreement 16-625-CA issued by the U.S. Forest Service, Rocky Mountain Forest and Range Experiment Station, Fort Collins, Colorado. Mr. Robert Dana was the technical monitor of the project. In addition portions of this research were supported by the U.S. Army Research Office-Durham under Contract DAAG 29-76-G-00105. Dr. Finn Bronner was the technical monitor for this project. Field data for the project were gathered over intensive measurement sites located in Leadville, Colorado. These sites were located on property leased by ASARCO, Incorporated, and by the Jacobson family, a private landowner.

Participating project personnel at various times included Dr. James A. Smith, Department of Earth Resources and Principal Investigator; Dr. Joe Berry, Yale University and formerly Research Associate in the Department of Earth Resources; Mr. Rick Heimes, Division of Water Resources, U.S.G.S. and formerly Graduate Research Assistant, Department of Earth Resources; Mr. Jon Ranson, Research Associate, Department of Earth Resources. Other project personnel included Mr. Dan Kimes, Graduate Research Assistant, Department of Earth Resources, Mr. Frank Itkowsky, Graduate Research Assistant, Department of Earth Resources and Miss Carol Conrad. Mr. Rick Heimes received a Master of Science degree for work related to project tasks and Chapters two through six are extracted from his thesis paper.

TABLE OF CONTENTS

CHAPTER		PAGE
1.0	INTRODUCTION	1
	1.1 The Mixture Problem	5
2.0	STUDY SITE	9
	2.1 Physical Description of Study Area	9
	2.2 Intensive Test Sites	12
3.0	INSTRUMENTATION AND MEASUREMENTS	17
	3.1 Tower Tramway Support System	17
	3.2 Instrumentation	18
	3.3 Data Collection Procedures	24
4.0	DATA REDUCTION	33
	4.1 Spectral Irradiance Estimation	33
	4.2 Calculating Spectral Reflectance	39
	4.3 Estimation of Scene Components and Proportions	39
5.0	ANALYSIS	45
	5.1 Scatter Plot Analysis	45
	5.2 Sun Angle Calculation	58
	5.3 Eigenvalue, Eigenvector, and Ellipse of Concentration Determinations	59
	5.4 Linear Regression Model	63
6.0	RESULTS AND DISCUSSION	71
	6.1 Scatter Plot Analysis	71
	6.2 Sun Angle Calculation	75
	6.3 Eigenvalue, Eigenvector, and Ellipse of Concentration Determination	76
	6.4 Linear Regression Model	77
7.0	CONCLUSIONS AND RECOMMENDATIONS	85
	References Cited	89
	Appendix A - Data Listings	91
	Appendix B - Program Listings	105

LIST OF TABLES

TABLE	DESCRIPTION	PAGE
1.	Regression equations to predict narrow band irradiance values from broad band irradiance measurements	36
2.	Basic statistics for measured and predicted irradiance values	38
3.	Summary of observations	43
4.	Coefficients for proportions of canopy and understory (M-3 data)	64
5.	Regression equations for M-3 and IH-1 site	79
6.	Comparison of regression and prediction R^2 values (August M-3 data)	81

LIST OF FIGURES

FIGURE	DESCRIPTION	PAGE
1.	General location of study area	10
2.	M-3 site viewed across meadow opening	13
3.	Study area with M-3 and IH-1 locations depicted	15
4.	IH-1 site	16
5.	Schematic of forest aerial tramway system	18
6.	Support cables and instrument cart suspended over M-3 site	18
7.	Control switching system	21
8.	Cart-mounted radiometer and two Hasselblad cameras	23
9.	Cart instrumentation suspended on support cables	23
10.	Basic components of Scene Recording Radiometer (SRR)	24
11.	Detector response as a function of angular field of view	26
12.	Broad band irradiance probe and $BaSO_4$ panel, and cart suspended $BaSO_4$ panel	28
13.	Sample spectral irradiance curves measured from $BaSO_4$ panel	29
14.	Plot of broad band irradiance versus narrow band (.5145μm) irradiance	34
15.	Measured irradiance versus percent difference between measured and predicted irradiance at .5145μm wavelength	37
16A.	Photographic record of composite forest scene (Pinus contorta)	42
16B.	Photographic record of composite understory scene	42
17(A-F).	M-3 site proportion of scene components versus reflectance at .675μm and .96μm bands	47 and 48
18(A-H).	IH-1 site proportion of scene components versus reflectance at .675μm and .96μm bands	49 and 50
19(A&B).	M-3 transect position versus reflectance at .675μm band and .96μm band	51 and 52
20(A&B).	IH-1 transect position versus reflectance at .675μm band and .96μm band	53 and 54

LIST OF FIGURES
(Continued)

FIGURE	DESCRIPTION	PAGE
21.	M-3 site; .675μm band reflectance versus .96μm band reflectance	56
22.	IH-1 site; .675μm band reflectance versus .96μm band reflectance	56
23.	M-3 site .675μm band reflectance versus .96μm band reflectance (canopy and understory categories)	57
24.	Ellipses of concentration (M-3 and IH-1)	61
25.	Ellipses of concentration (Canopy, understory, all M-3)	62
26.	Wavelength versus understory proportion coefficients (4 data groups)	70
27.	Wavelength versus canopy proportion coefficients (4 data groups)	70

1.0 INTRODUCTION

The research efforts described in this report were funded by the Rocky Mountain Forest and Range Experiment Station under Cooperative Agreement 16-USC and, in part, by the U.S. Army Research Office-Durham under Contract DAAG 29-76-G-00105. The specific objectives of this study as described in the study plan submitted to the U.S. Forest Service include:

1. To develop a digitized spectral reflectance data base for a montane/subalpine area. Vegetation and soil type, topography, sun angle, and radiometric data will be included.
2. To develop a canopy reflectance model that will be applied to forest and forest/grass mixtures to evaluate spectral variability resulting from topography, sun angle, and mixtures.
3. Signature extension techniques will be reviewed and recommendations will be made for potential implementations.

Objective one has been accomplished. A digitized data base including scene components (vegetation understory, soil and rocks), sun angle, site description, and reflectance measurements was compiled through the period August 1, 1976 to December 30, 1976. These data are included in Appendix A in this report.

Objective two has been completed with respect to developing canopy reflectance regression models to evaluate spectral variability resulting from mixtures of forest components. This work was the subject of a Masters thesis by Mr. F. Heimes, and the bulk of this report is extracted from his thesis. A process-oriented modeling effort has been initiated to investigate the interaction of light with forest canopies and scene components. This will permit a better analysis of sun angle and topographic

effects on spectral characteristics.

Objective three has been addressed. A discussion of parameter inversion strategies for the mixture problem was included in the December Quarterly Progress Report. In general, there are two fundamental concepts of signature extension. The first is to seek a transformation, which maps radiance values from state i to state j where i and j correspond to change in scene reflectance, sun angle, or atmospheric condition. Scene reflectance changes can depend on a variety of factors such as scene proportions, status, and underlying topography. Usually the transformation is assumed to be Affine, that is the radiance at state i is assumed to be linearly related to that of state j,

$$\text{i.e.,}\quad N_j = \alpha_{ij} N_i + \beta_{ij} \qquad (1)$$ (wavelength by wavelength)

where N_{ij} = scene radiance for state i or j

α_{ij} = diagonal matrix of multiplicative correction coefficient

β_{ij} = diagonal matrix of additive correction coefficient terms.

The correction coefficients can be estimated from either empirical or modeling considerations. In general, the coefficient terms may be related to ground radiance and path radiance.

Given an Affine transformation such as (1) above, one can either transform individual radiance values from one scene segment (condition or state) to another or transform the training signatures as follows:

$$\begin{aligned} \underline{M}_j &= \alpha_{ij}\, \underline{M}_i + \beta_{ij} \\ \underline{\Sigma}_j &= \alpha_{ij}\, \underline{\Sigma}_i\, \alpha_{ij}^T \end{aligned} \qquad (2)$$

where (M,Σ) represent the mean vector and covariance matrix for the particular training category.

Generally, this approach to signature extension has met with limited success primarily because of the difficulty of defining suitable α,β terms which are stable over reasonable spatial or temporal ranges.

A second concept of signature extension is that of identifying suitable scene stratifications in which classifications may be performed. That is, analysis of signature variation with topography for particular conditions might indicate that the scene should be stratified into the following four slope categories; 0-30%, 30-40%, and greater than 40%. All scene elements belonging to these strata should be classified separately. An alternative variation of this concept is to develop transformations which will reduce or associate various spectral clusters, arising, for example, from unsupervised clustering, into smaller sets.

Further field work and supporting aircraft data are required to evaluate specific approaches. In this study, attention was placed on variations of scene reflectance for different conditions, primarily scene component proportions. This is called the mixture problem.

1.1 The Mixture Problem

The "mixtures problem" has been and continues to be a nemesis to individuals in the remote sensing community who are interested in mapping or classification of vegetation communities. This is especially true when classifications are attempted using small scale imagery such as that provided by the LANDSAT satellites. In the case of LANDSAT, the resolution element (smallest area that can be resolved) is approximately 1.1 acres (.45 hectares) at the earth's surface. This resolution element is large enough in size that it may contain two or more vegetation types; which would be termed a mixture.

Classification of vegetation types using small scale imagery has been quite successful in areas where the vegetation cover is uniform and homogenous. Coggeshall and Hoffer (1973) report that "accurate classification of deciduous and coniferous forest cover can be achieved." Leschack (1971) identified and mapped the distribution of five different forest types in Columbia, Panama, and Peru. In areas where the vegetation is not homogenous or at boundaries between vegetation types, classification accuracies are greatly reduced. Driscoll and Francis (1970) stated that "in areas of heterogenous vegetation types, a single mapping unit defined by the photo image element, may consist of two or more plant community types..." Basically the larger a resolution element is the greater the probability that it will contain two or more vegetation types. A resolution element containing a mixture of vegetation types exhibits reflectance characteristics that are different from the individual vegetation classes that comprise the mixture. In machine-assisted classification, a characteristic reflectance curve (spectral signature) can be developed for a homogenous vegetation type and then used for its

identification. It is not possible to reliably develop a spectral signature for a mixture situation because the proportions and types of vegetation may vary from one resolution element to another.

Two general directions have been taken in approaching the mixtures problem. One approach treats the classification technique, while the other approach attempts to model the relationships between the types and proportions of vegetation within a resolution element and the spectral response from that element.

In the first approach either of two basic classification techniques are generally employed: (1) classifying a resolution element as a single vegetation type or class using some decision function or (2) thresholding out the resolution elements that do not have a signature characteristic of an individual vegetation type or class. This procedure results in leaving these elements unclassified.

The modeling approach has various levels of complexity. Mead (1974) in his Masters thesis utilized regression models to relate mean spectral response from ponderosa pine forests to tree cover density. Pearson (1973) and Ranson (1975) investigated a simple least squares approach to the mixtures problem and suggested some practical applications of this method. Pace and Detchmendy (1972; 1973) developed the following least squares (regression) approach for relating vegetation components to scene reflectance.

Assuming r materials per resolution element and m spectral channels:

$$d_i = \sum_{j=1}^{r} S_{ij} a_j + n_i \quad i = 1,2,\ldots,m$$

where

d_i = observation in the i^{th} channel

a_j = the fractional area or proportion, covered by the j^{th} component

s_{ij} = i^{th} component of the basis vector for the j^{th} mixture component

n_i = a noise term in the i^{th} channel.

In matrix form the equation is:

$$\underline{D} = \underline{SA} + \underline{n}$$

subject to: $\sum_{j=1}^{r} a_j = 1$; $a_j \leq 0$ all j.

A somewhat more complex approach which expands on the least squares solution involves parameter (component proportion) estimation using maximum likelihood procedures (Horwitz et al., 1971).

It is evident from the above discussion that there are several approaches to solving the mixtures problems. All of these approaches have several underlying assumptions, which, in fact, have not been evaluated. The most critical assumption common to the models discussed is that the resolution element consists of a flat surface. Furthermore, it appears that it is difficult to evaluate the solutions to these models because of the lack of well-defined data sets in which both the observations, D, and the proportions, A, are known simultaneously with reasonable confidence.

It is the purpose of this study to further evaluate the applicability of the least squares approach (Pace and Detchmendy, 1972; 1973) utilizing a well defined data set. Observations D and proportions A are obtained by simultaneously acquiring radiometer data and a photographic

record of the scene. In addition, this study will address the consideration of three dimensional structure within the scene and its effect of spectral response. Three dimensional structure and sun angle relative to the scene are considered indirectly by including a scene component consisting of a proportion of shadowed areas.

2.0 STUDY SITE

The study area is situated immediately southeast of the city of Leadville, Colorado (Figure 1). This location, called "Iron Hill", was selected because of its diversity and the fact that other related studies were currently in progress in that area. Iron Hill was the site of extensive mining activities during the late 1800's and early 1900's. Soils in much of the area still contain very high concentrations of Lead and Zinc as a result of mining spoils and ore bodies near the surface. These anomalous concentrations of Lead and Zinc prompted the initial selection of this area in support of efforts to investigate stress effects on vegetative reflectance characteristics. The ultimate goal of this related work is to develop techniques to enhance subtle changes in reflectance characteristics of a forest scene in response to stress factors. The mining and related activities which took place around the turn of the century have resulted in considerable diversity of cover types and density. This factor made the area equally desirable as a test site to investigate the relationship between mixtures and scene reflectance characteristics.

2.1 Physical Description of Study Area

Elevation in the test area ranges from about 10,400 ft. (3,170 m) to slightly over 11,000 ft. (3,353 m). Average annual temperature is about 36 F (2^{o}C) with an average annual precipitation of between 19" (48 cm) and 25" (64 cm). Slopes in the study area range between 0 and 50 percent.

The geology of the area is Precambrian gneiss and granite overlain by about 500 feet (152 m) of Cambrian through Mississippian age dolomite,

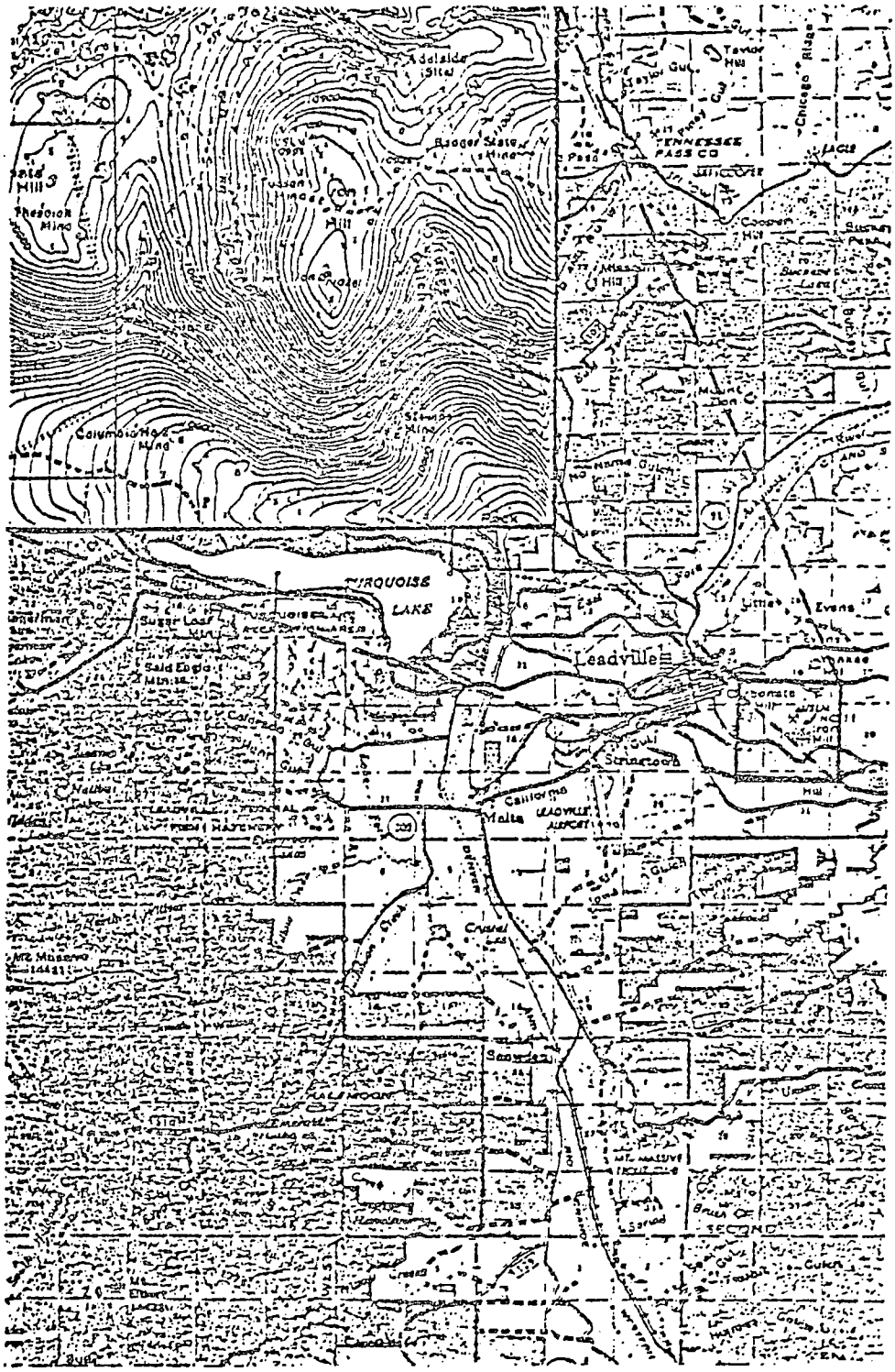

FIGURE 1. General location of study area

shale, and sandstone (Behre, 1953). These rocks have been intruded by Cretaceous-early Tertiary quartz monzonite sills, dikes, and stocks. Faulting has provided control on emplacement of igneous rocks in some places.

Soils in undisturbed areas are predominantly gravelly sandy loam which are well developed and moderately deep. Soils in disturbed areas, which are primarily the result of mining activities, are widely variable in texture, depth, and mineral content.

Vegetative cover in undisturbed areas is primarily lodgepole pine (Pinus contorta) with lesser amounts of Aspen (Populus tremuloides), Engelmann spruce (Picea engelmanii), subalpine fir (Abies lasiocarpa), and blue spruce (Picea pungens). Disturbed areas and understory in more open forest stands include Juniper (Juniperus communis), sagebrush (Artemisia) and grass meadow openings which are primarily fescue (Festuca), brome (Bromus), sedge (Carex) and rush (Juncus).

2.2 Intensive Test Sites

One primary and one secondary intensive test site within the general area were utilized for this study. The primary site (M-3) was selected for the majority of the data collected in conjunction with the mixtures experiment. This site was chosen because it provides a lodgepole pine canopy with variable canopy density ranging from about 80% crown closure to a completely open, grass-covered clearing (Figure 2). Thus, there is a wide range of proportions for a limited number of different scene components contained within the site.

The M-3 site is located in the northeastern section of the Iron Hill area, immediately adjacent to the old Adelaide town site (Figure 3). The town, typical of many small mining communities, was abandoned when the mining activity was terminated in the late 1920's. All that remains of the town are the remnants of several foundations. However, activity surrounding the town led to a regeneration of lodgepole pine interspersed with a number of large meadow openings. The age of the stand in this area is between 30 and 50 years. Average height of the stand is approximately 20 feet (6.1 m). The M-3 transect is a straight line of 150 feet (45.7 m) which gradates from a relatively dense lodgepole stand to an open meadow area and back into a lodgepole stand. The meadow opening is approximately 40 feet (12.2 m) in diameter. Grass, like that in the meadow opening, also makes up the majority of the understory along the remainder of the transect. The transect orientation is 060° to 240°. Slope and aspect along the transect are relatively constant at 5% at 045° along the entire length of the transect. Elevation at the site is about 10,900 feet (3,322 m). Soils in this area are sandy loam in the upper horizons changing to gravelly sandy loam at the

FIGURE 2. M-3 site viewed across meadow opening

depth of about 1 - 1½ feet (30-46 cm). This area is not subject to potential mineral induced stress as discussed earlier.

The second site (IH-1) was selected as an alternate location to evaluate potential extension of the modeling techniques developed on the M-3 site. This site is generally more open than the M-3 site, with less variability in density. Crown closure averages 30-40%. The range of proportions of scene components is reduced at this site but the number of components is increased. The IH-1 site is located approximately 400 feet (122 m) NNE of the summit of Iron Hill, at an elevation of 11,000 feet (3,353 m) (Figure 3). This area is also lodgepole pine, although the density of the stand is considerably less than that of the M-3 site. Understory in this location is made up primarily of bare soil, and litter, and small clumps of sage interspersed with numerous white rock fragments which are a result of weathering of the parent material, the Pando porphyry (Figure 4). The IH-1 transect is a straight line of 150 feet (45.7 m) which maintains a relatively constant stand density along the entire distance. The transect orientation is 090° to 270° . Slope and aspect remain a relatively constant 3% at 070° along the entire length of the transect. Soil in this area is gravelly sandy loam with numerous rocks. This location is underlain by a lead/zinc orebody at about 200 feet (61 m). Based on information gathered from geochemical sampling of soils and trees, it is possible that this site may be under some stress from anomalous concentrations of Lead and Zinc.

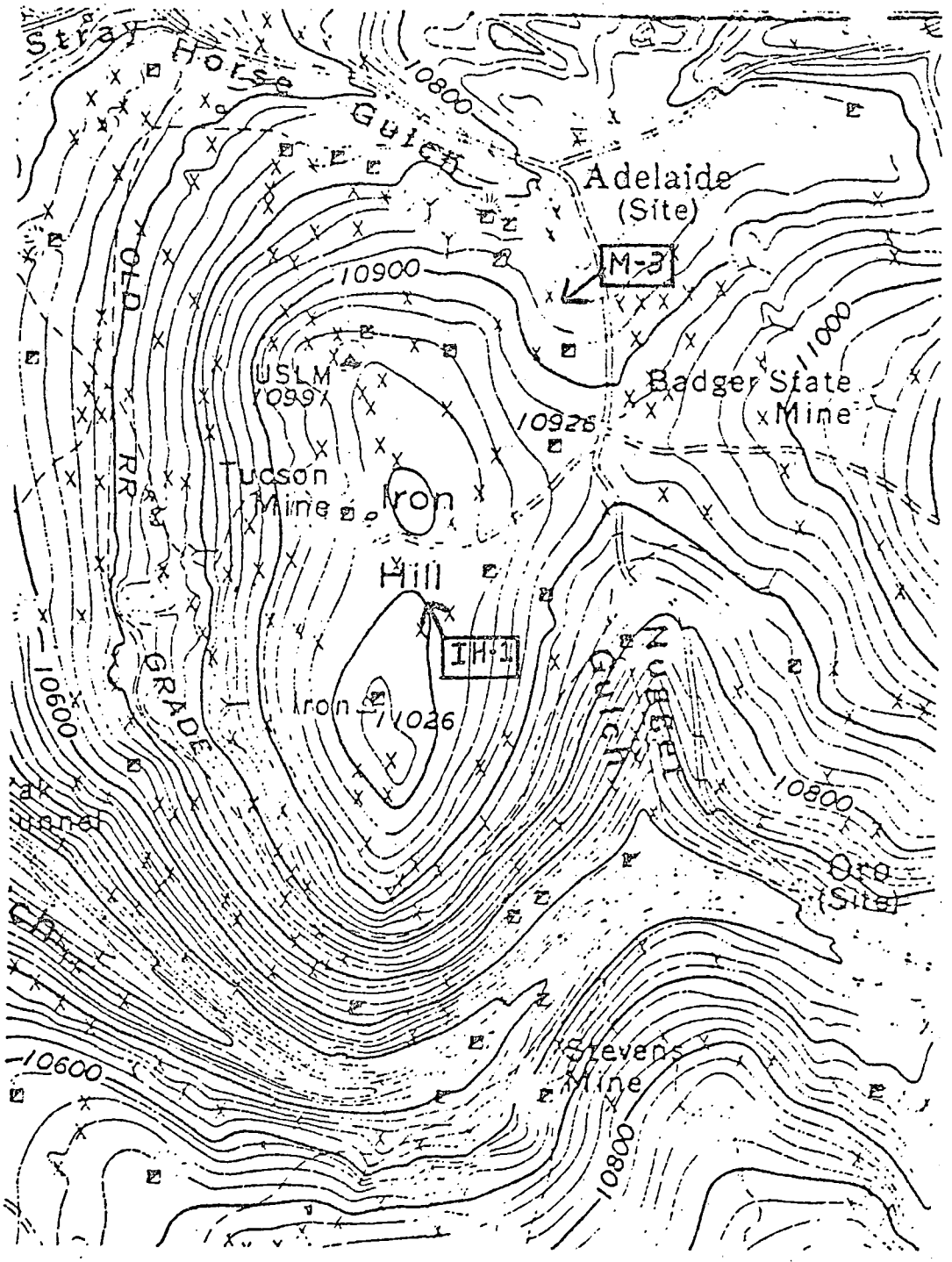

FIGURE 3. Study area with M-3 and IH-1 locations depicted

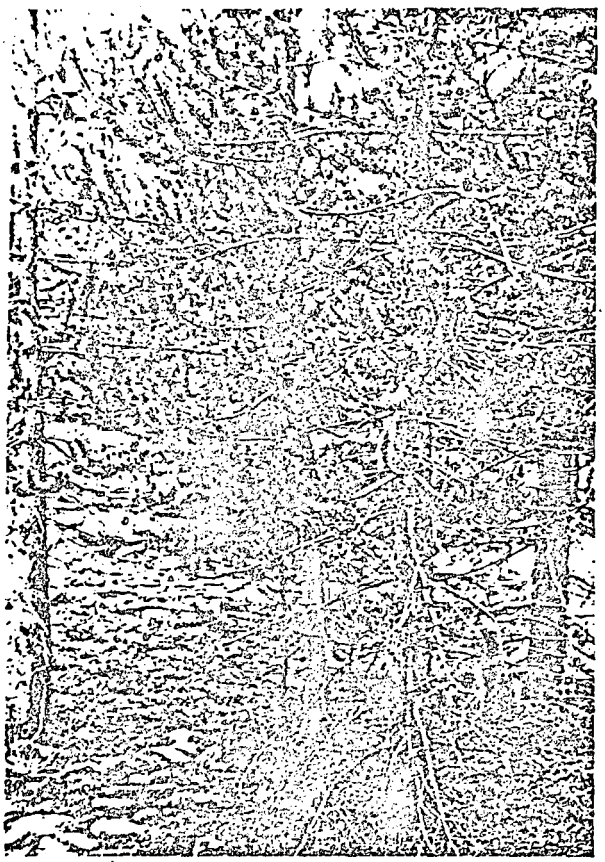

FIGURE 4. IH-1 site

3.0 INSTRUMENTATION AND MEASUREMENTS

Instrumentation for this project had to be specially designed to meet the unique field data needs of having radiometric measurements with an exact record of the scene. In addition, the data collection platform had to be located above the forest canopy and still have a small enough field-of-view to facilitate scene component measurement. An aerial tramway system and a cart-mounted camera and radiometer unit were developed to meet these requirements.

3.1 Tower Tramway Support System

The basic components of the tramway system are support towers, support cables, driving cables and winch mechanism, and an instrument cart (Leonard and Eschner, 1968), (Burroughs, 1971). Figure 5 schematically describes the general makeup of the tramway systems used in conjunction with the mixtures experiments.

The towers which support the ends of the aerial tramway are of the type commonly used to hold television antennae. Each section of the triangular steel tower is about 12 inches (30.5 cm) on a side and 10 feet (3.05 m) long with the capability to support 300 pounds (136 Kg) when properly gauged. The tramway transect consists of two 50 foot (15.2m) (5 section) towers positioned 150 feet (45.7 m) apart. Each tower is anchored by 3 cables attached at the 30 foot (9.1 m) level and by an additional 3 cables at the 50 foot (15.2 m) level. These anchor cables are attached to the base of surrounding trees where feasible and to concrete anchors set in the ground when trees are not available. The two towers are interconnected by a pair of support cables on which the instrument cart is suspended (Figure 6). The

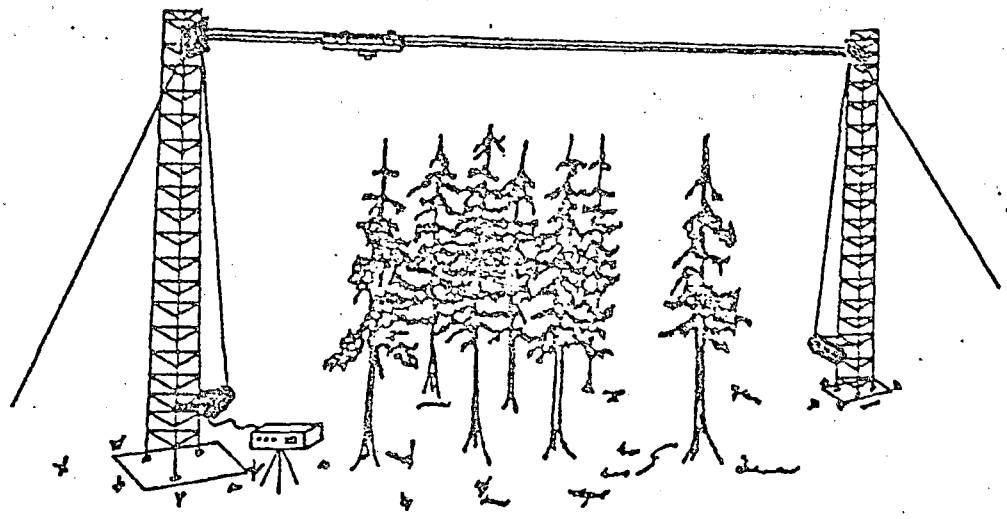

FIGURE 5. Schematic of Forest Aerial Tramway System

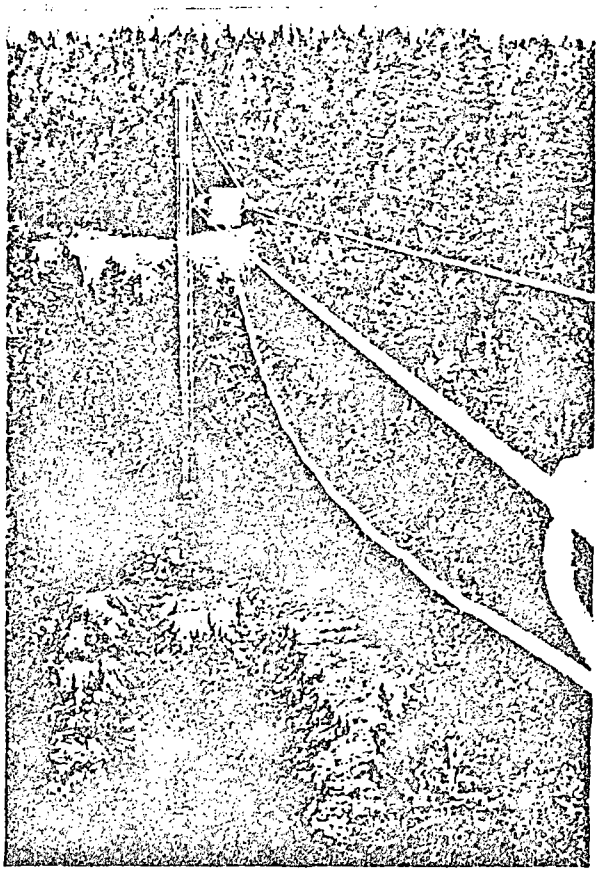

FIGURE 6. Support cables and instrument cart suspended over M-3 site

support cables are connected to the towers using a turnbuckle assembly which allows adjustment of the cables to insure leveling of the instrument cart. The drive mechanism for the instrument cart consists of two cables, one attached to either end. One cable serves as a drive cable in one direction. This cable is attached to a winch system located at the base of one of the towers. The other cable, which is 6 strand paired shielded electrical wire, serves as a drive cable in the other direction and, in addition, provides the electrical connection between the instrument cart and control equipment on the ground. This two cable drive system combined with distance marks on both cables allows relatively precise positioning of the cart at points along the transect.

A tramway system consisting of two 50 foot (15.2 m) towers and related equipment can be disassembled, moved to a new location, and reassembled by a four man team in a period of 4-6 hours. This flexibility allows data collection over a number of different locations without the cost associated with several different permanent tramway systems. The only permanent installations at each site are the two concrete bases and associated anchor points.

The two tramway systems used in this study were positioned at each of the intensive sites, M-3 and IH-1, as described in Section 2.2.

3.2 Instrumentation

The primary tramway data collection system is composed of 3 basic units with interconnecting electrical leads. The three units consist of 1) a ground control unit, 2) a broad-band single probe irradiance monitor, and 3) a cart mounted combination narrow-band radiometer and camera unit.

The ground control unit consists of a control/switching system and a digital photometer. The switching system allows remote selection of each of 6 filter positions on the cart-mounted radiometer. The control unit contains a two position selector switch which allows monitoring of either the broad-band irradiance probe or the cart-mounted radiometer. A camera switch on the control unit allows remote shutter operation of cart-mounted cameras. A J-16 digital photometer (Tektronix, Inc., 1972) is integrated with the control unit to provide a readout of signals obtained by the cart-mounted radiometer or the broad-band irradiance probe. The control/switching unit is powered by a small twelve-volt battery. The control/switching system and J-16 photometer are housed in a portable, shock resistant steel case (Figure 7).

The broad-band irradiance monitor utilizes a single probe positioned above a $BaSO_4$ panel. The $BaSO_4$ panel consists of a flat panel covered with Kodak-Eastman White Reflectance Paint (Catalog #6080), which is a composition of $BaSO_4$, binder and solvent. This coating is characterized by high stability and nearly perfect diffuse (Lambertian) reflectance of greater than 98% in visible and near infrared wavelengths. The panel is positioned atop one of the towers in a level position clear of any obstructions. The silicon cell detector is positioned to view the panel from a distance of approximately 6 inches (15.2 cm) at an angle of about 45°. The detector is sensitive to wavelengths between .35μm and 1.1μm. The broad-band irradiance monitor is connected to the ground control unit by an individually shielded 6 pair instrument cable.

The cart-mounted instrumentation normally includes a scene recording radiometer and 2 additional Hasselblad EL500 cameras (Figure 8). Removal of the radiometer allows mounting of up to four of the

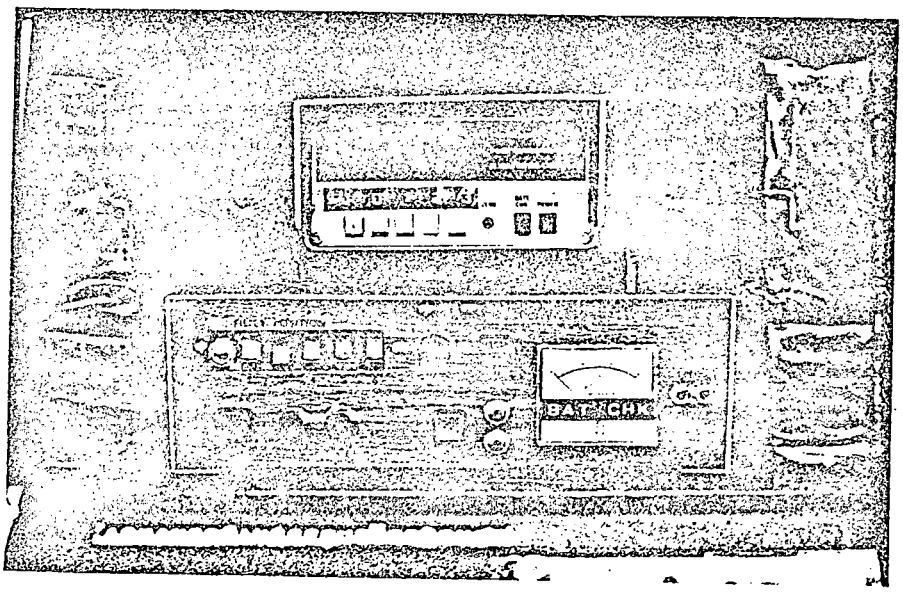

FIGURE 7. Control/switching system

EL500 cameras on the cart systems. The cart-mounted instrumentation is connected with the ground control unit by individually shielded 6 pair instrument cable. The instrument cart rides on the two support cables using four wheels, one at each corner of the cart. A pair of quick links attached to the side of the cart is used as a safety system to retain the cart on the support cables (Figure 9). As discussed in Section 3.1, cart positioning is controlled by the instrument cable attached to one end and a drive cable attached to the other end.

The scene recording radiometer system is essentially a remote controlled filter wheel radiometer interfaced to a Hasselblad EL 500 camera (Figure 10). The functions of the system are four fold: 1) detection of the spectral signal, 2) partitioning the signal into wavelength bands, 3) controlling the filter wheel position, and 4) photographing the scene.

The radiometer system uses a silicon detector directed towards the viewing glass of the camera. The optics of the camera define the instrument's limiting field-of-view. This allows adjustment of the radio-meter field-of-view by varying the camera's lens system. Sharp definition of the field-of-view of the instrument is further achieved by overlaying a circular mask on the viewing glass. The diameter of the mask was constructed to be slightly smaller than the physically constrained field-of-view of the detector when interdicted by an interference filter. This constrained field-of-view was measured by mounting the instrument on a goniometer and rotating it about the optical axis of the camera, while exposing it to a narrow beam of light. An interference filter centered at 6328°A was used to accommodate a helium gas neon laser light source. The relative output signal was measured at

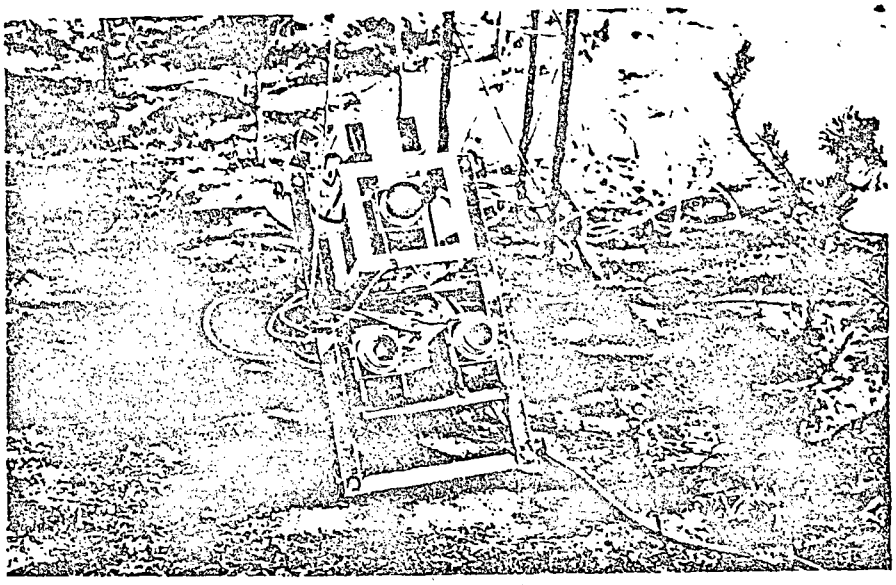

FIGURE 8. Cart mounted radiometer and two Hasselblad cameras

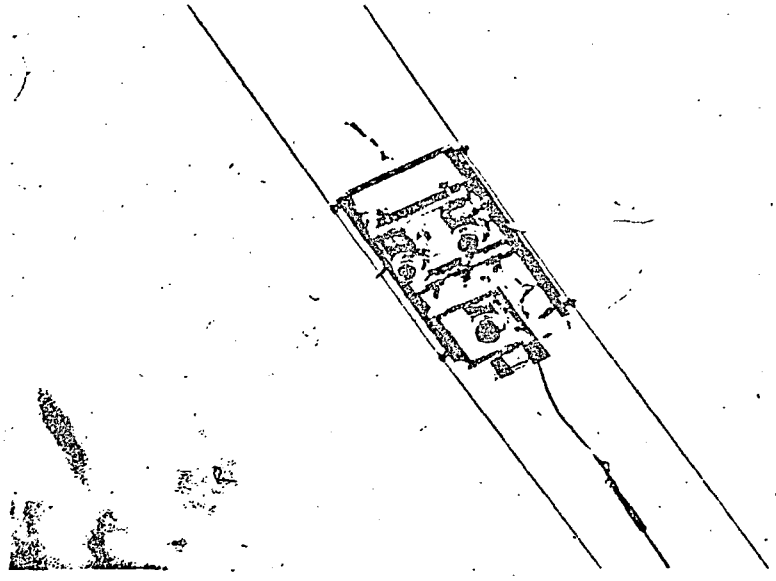

FIGURE 9. Cart instrumentation suspended on support cables

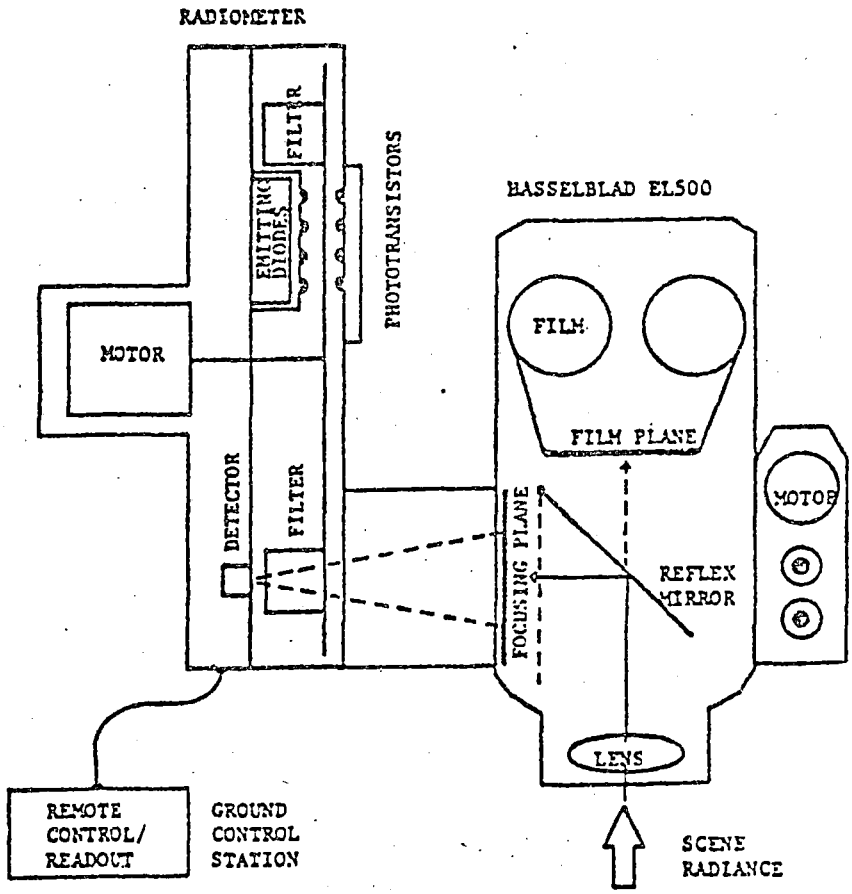

FIGURE 10. Basic Components of Scene Recording Radiometer (SRR)

2.5° deflection angle increments and the half-peak angular field-of-view was determined to be 5.0° (Figure 11). Companion photographs were made for each measurement. These were used in transcribing the instrument's actual field-of-view to photographic negatives of field scenes.

Signal detection at discrete wavelength bands is achieved by successively rotating interchangeable interference filters that interdict the view of the silicon detector. Filter wheel positioning is controlled by binary coding holes in the filter wheel disk, which are electronically registered by a bank of opposing light-emitting diodes and phototransistors. A low voltage DC motor is used to rotate the six position filter wheel. Filter positions are remotely selected from the ground control unit. The filter set used for the mixture experiments consisted of interference filters with center wavelengths at .4600, .5145, .5500, .6750, .8000 and .9600μm. Half width bandpasses are approximately 100 A with 60% minimum peak transmission.

Cameras mounted on the instrument cart, including the one interfaced with the radiometer, allow remote shutter operation and automatic film advance using the ground control unit. Focus, shutter speed and f-stop must be manually set for each camera.

3.3 Data Collection Procedures

Four types of data were collected in conjunction with this experiment. These included 1) incoming broad-band and spectral irradiance, 2) scene spectral radiance, 3) broad-band black and white photographs and physical stand characteristics.

Incoming broad-band irradiance measurements were obtained using the $BaSO_4$ panel and broad-band detector as discussed in Section 3.2.

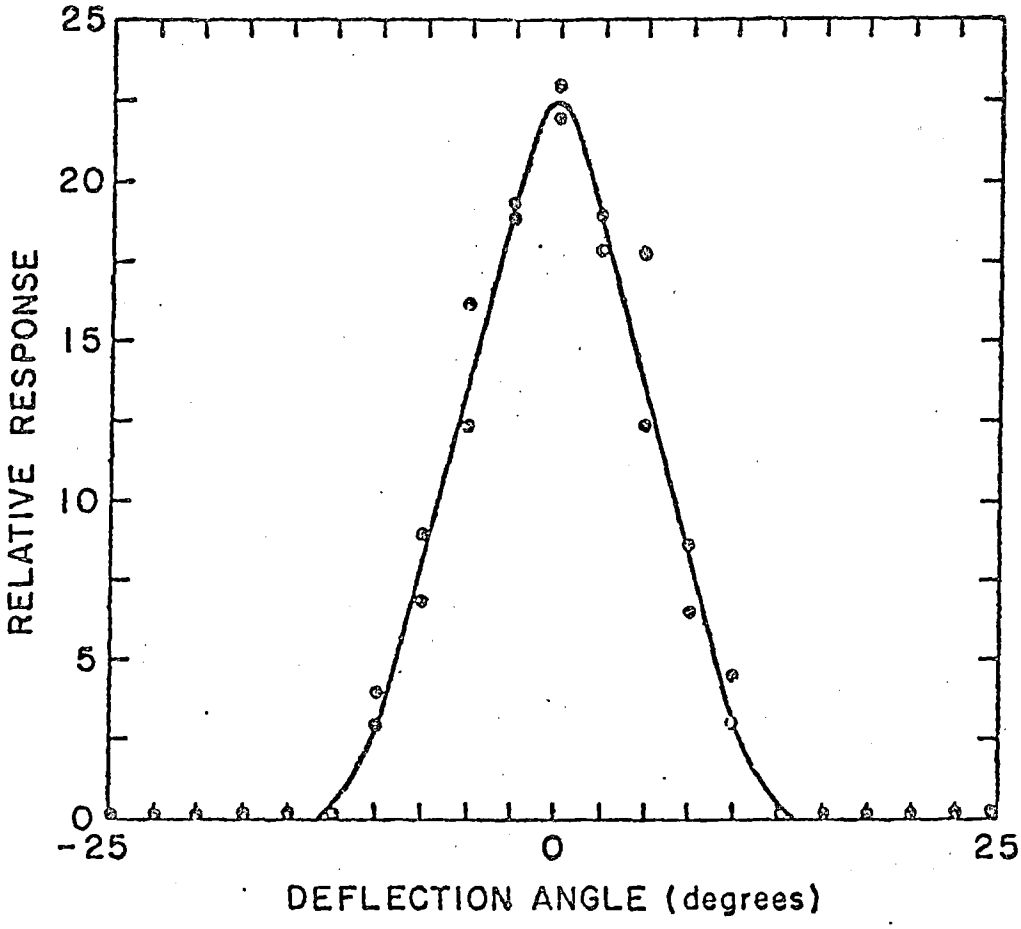

FIGURE 11. Detector response as a function of angular field-of-view

Incoming spectral irradiance measurements were made by suspending a second $BaSO_4$ panel in the field-of-view of the Scene Recording Radiometer (SRR) (Figure 12). Readings of each of the filters provided irradiance data in the six spectral bands. Several sample spectral irradiance curves are presented in Figure 13. The dip in irradiance at the .55 μm wavelength is also indicated in Figure 4-3 (Reeves et al., 1975). The irradiance dip at .55 μm may also be a function of transmission characteristics of the filter. Spectral irradiance data is required for calculating reflectance values from scene radiance readings. These calculations are described in Section 4.2. Attaching the $BaSO_4$ panel to the SRR required positioning of the instrument cart immediately adjacent to the support tower to allow personnel access. Irradiance values fluctuate sufficiently to require a measurement of irradiance for each set of scene radiance data recorded. This method is thus unsuitable for estimating spectral irradiance at points along the transect. The method would require returning the instrument cart to the tower to attach and detach the $BaSO_4$ panel following the collection of each scene radiance data set.

It was decided that broad-band irradiance data could be used to predict spectral irradiance with reasonable accuracy. Methods used for this prediction and the accuracy of the results are discussed in Section 4.1. Procedures used for collection of irradiance data involved obtaining spectral irradiance readings using the SRR and $BaSO_4$ panel at the beginning and the end of each set of measurements along the transect. Irradiance values for measurements conducted at points along the transect were monitored by the broad-band detector and $BaSO_4$ panel positioned atop one of the support towers. Data collected using this double sampling

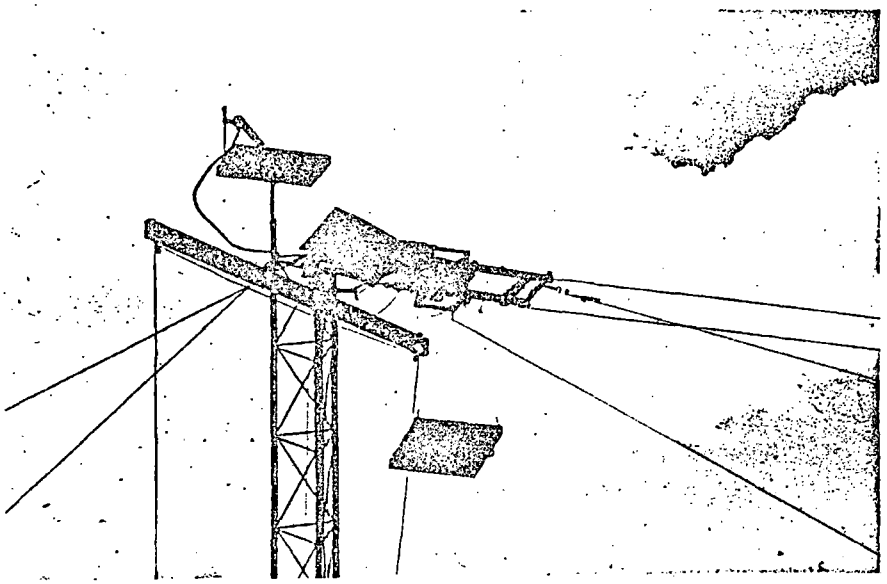

FIGURE 12. Broad band irradiance probe and $BaSO_4$ panel, and cart suspended $BaSO_4$ panel

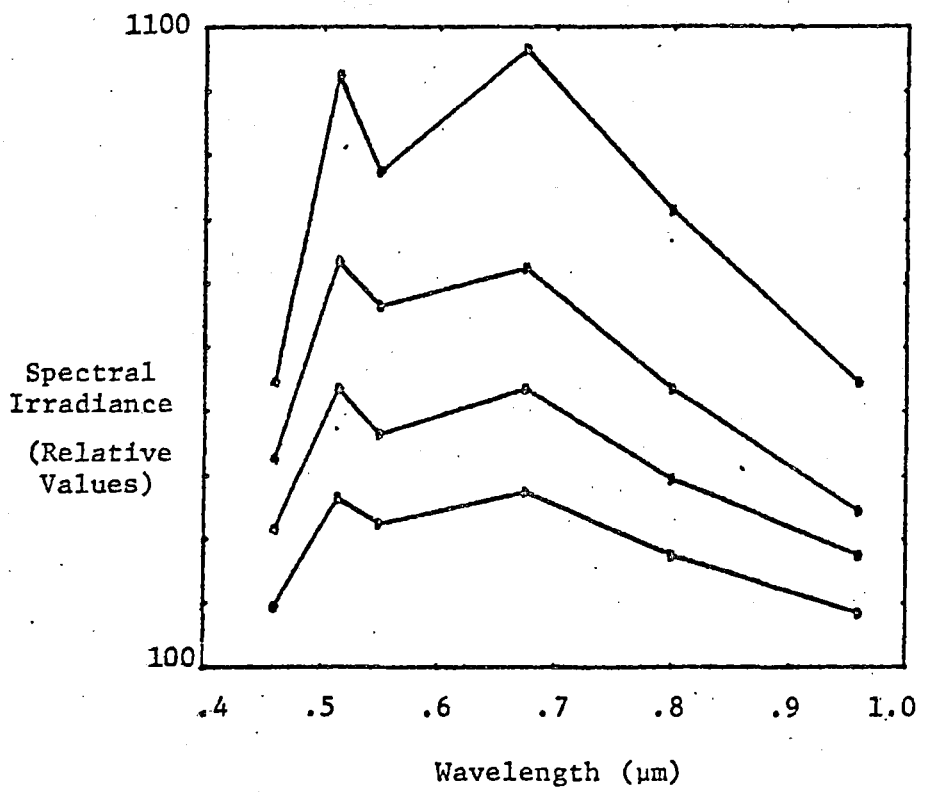

FIGURE 13. Sample spectral irradiance curves measured from $BaSO_4$ panel

procedure was used to develop the methods for predicting spectral irradiance values from broad-band irradiance data. This prediction technique was used to provide spectral irradiance estimates for measurement points along the transect where actual measurement of the values was not feasible.

Procedures used in the collection of scene radiance data from the tramway-mounted SRR system were designed to support the mixtures experiment directly.

Typical procedures involved the measurement of a scene radiance data set at 10 foot (3 m) increments along the total length of the transect. Positioning of the instrument at the ten foot (3 m) intervals was accomplished using distance markers on both drive and instrument cables. Collection of a scene radiance data set for a specified point consisted of the following procedures: 1) measurement of the broadband irradiance, 2) measurement of scene radiance for each of the 6 spectral bands described in Section 2.3, 3) a repeat measurement of broad band irradiance and 4) acquisition of a black and white photograph of the scene. Photographs were obtained for subsequent determination of proportion of scene components. This procedure is described in detail in Section 4.4.

Data collection periods for scene radiance varied considerably. Typically, the majority of the data was obtained during the morning hours as a result of extensive cloud development beginning about mid-day and continuing through the afternoon. However, the timing of cloud formation varied from day to day. Some days the cloud cover prevented collection of any data while several days remained relatively cloud free allowing extensive data collection periods.

Physical stand characteristics collected for the two transects, M-3 and IH-1, included tree height, age, and diameter at breast height (DBH). The sampling area for these measurements included everything contained within 35 feet (10.7 m) either side of the center line of the 150 foot (45.7 m) transect. Tree height and DBH were recorded for all trees within the area that were in excess of 8 feet (2.4 m) in height. Measurements of tree height and DBH were obtained using a clinometer and a DBH tape respectively. Age of trees in the stand was determined for approximately 10 percent of total trees measured for height and DBH. Age was determined by counting growth rings in a core obtained at breast height. A summary of these physical stand characteristics for each site, is contained in Appendix A. In subsequent analyses, these physical stand characteristics are not actually utilized. However, they are included in Appendix A for completeness in relation to the site description.

4.0 DATA REDUCTION

This section provides a description of techniques used for basic data reduction and for determination of parameters which were not directly measured during data acquisition. Included in this section is a discussion of 1) Regression techniques employed for predicting spectral irradiance values from broad-band irradiance data 2) Methods for calculating spectral reflectance and 3) Procedures utilized in estimating scene component proportions from black and white negatives.

4.1 Spectral Irradiance Estimation

Initially, a simple percentage increase for estimating spectral irradiance was evaluated. In this approach the percentage change in broad-band irradiance was applied directly to each of the spectral irradiance values. This procedure was found to be unsuitable because the spectral irradiance responses for different wavelengths vary by different percentage amounts for a given change in broad-band irradiance. Evaluation of paired data points indicated that a strong linear relationship existed between broad band irradiance values and values obtained from a specific spectral band (Figure 14). This relationship was evident for each of the six spectral bands within the range of the data that was acquired.

A simple linear regression model was employed to predict spectral irradiance values using broad band irradiance values as the independent variable. Separate regression equations were developed to predict irradiance values for each of the six spectral bands. Thirty seven pairs of data points were used to develop each of the regression equations. These data points were collected during a period from August

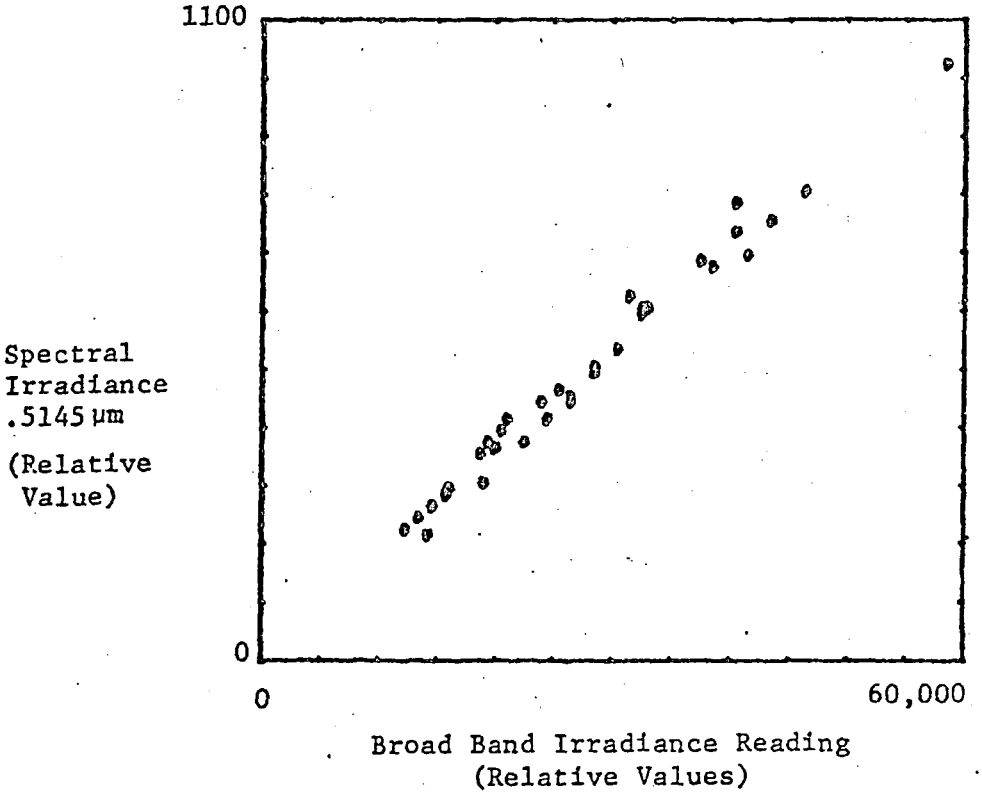

FIGURE 14. Plot of broad band irradiance versus narrow band (.5145µm) irradiance

through September 1976. The six regression equations and the R^2 values for each are presented in Table 1. The R^2 value is a numerical representation of the goodness of fit of the regression model (Draper and Smith). R^2 measures the proportion of total variation which is explained by the regression.

Analysis of the residuals plotted versus both the dependent (spectral band) and the independent (broad band) variables displayed a random distribution. This would indicate that deviations of data about the regression line are not directly related to the values of either the dependent or independent variables. However, additional analysis, calculating percent difference between measured spectral irradiance values and predicted spectral irradiance values indicated a larger percent difference between the two for the lower irradiance values. This was true primarily for the visible wavelengths. Figure 15, which is a plot of percent difference between measured and predicted irradiance values for the .5145μm band, is a good example of this trend. Based on this trend, data points which would use irradiance values from the lowest 10% of the data range were removed from consideration in subsequent reflectance calculations. Table 2 presents the mean, variance, standard deviation, standard error of the prediction and the average percent difference between measured and predicted spectral irradiance values for each band. Tests of the sensitivity of spectral reflectance values to the average percentage error in prediction of spectral irradiance indicates a direct transfer of the error. For example, if there is a 4% difference between measured and predicted spectral irradiance, then this would result in a 4% difference between the reflectances calculated using each of these two irradiance values. The standard error of prediction is

TABLE 1

Regression equations to predict narrow band irradiance values from broad band irradiance measurements.

Band 1 = .4600um 100 A Band Width
Band 2 = .5145um 100 A Band Width
Band 3 = .5500um 100 A Band Width
Band 4 = .6750um 100 A Band Width
Band 5 = .8000um 100 A Band Width
Band 6 = .9600um 100 A Band Width
Broad Band = .35um - 1.1um

Band 1 = 3.0813 + .0099 (Broad Band)

r^2 = .98

Band 2 - 8.5896 + .0176 (Broad Band)

r^2 = .98

Band 3 = 14.2368 + .0152 (Broad Band)

r^2 = .98

Band 4 = 29.7783 + .0171 (Broad Band)

r^2 = .97

Band 5 = 22.2218 + .0128 (Broad Band)

r^2 = .97

Band 6 = -8.6109 + .0091 (Broad Band)

r^2 = .95

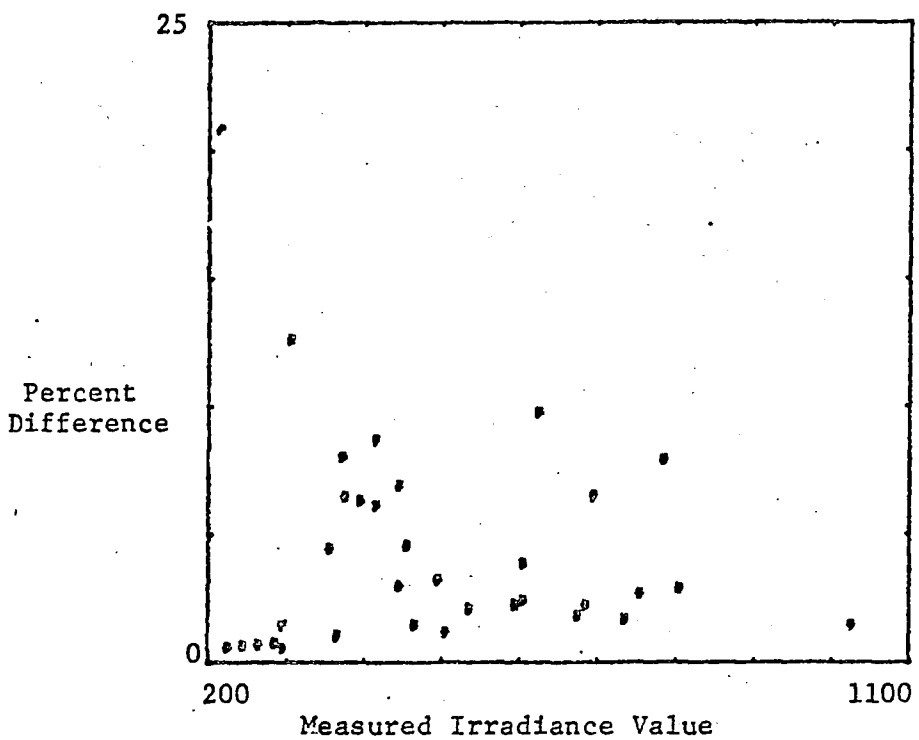

FIGURE 15. Measured Irradiance versus percent difference between measured and predicted irradiance at .5145μm wavelength.

TABLE 2. Basic statistics for measured and predicted irradiance values

Channel	Mean	Variance	Standard Deviation	Standard Error of Prediction	Mean % Difference Measured vs Predicted
Broad Band	27658.1	112657432.4	10614.0	--	--
.4600 um	277.4	11333.4	106.5	16.2	4.7
.5145 "	496.1	35626.6	188.8	25.4	4.1
.5500 "	435.4	26606.1	163.1	22.3	4.3
.6750 "	503.1	34065.8	184.6	33.2	5.4
.8000 "	374.7	18901.7	137.5	22.7	5.0
.9600 "	242.8	9750.9	98.7	21.3	7.2

essentially a measure of the standard deviation of the residuals. The error estimates presented in Table 2 are in general agreement with estimates obtained by Silvestro (1969) in his study on Multispectral Photographic Determination of Reflectance. In his study, Silvestro also employed a double sampling procedure to use total broad band irradiance to predict spectral irradiance for .6 and .8μm wavelengths.

4.2 Calculating Spectral Reflectance

Relectance is the ratio of scene radiance to incoming irradiance. Spectral reflectance is calculated by dividing the scene radiance for a specific wavelength by the corresponding irradiance for the same wavelength. All spectral irradiance values used for calculation of reflectance data were computed using the regression equations presented in Table 1.

4.3 Estimation of Scene Components and Proportions

The SRR's capability of providing a photographic record of the exact scene for which radiometric data is acquired allows comparison of composite scene reflectance data with primary scene components. Scene components refer to the physical components such as various overstory and understory types (mixtures) plus the additional factor of shadowing caused by the three dimensional structure of the scene. The primary scene components defined for this study were selected based on their spectral separability from one another and their potential contribution to the composite scene reflectance.

Due to the distinct difference between the M-3 site and the IH-1 site, as discussed in Section 2.2, different primary scene components were selected for each of the sites. The M-3 site is essentially a

lodgepole pine overstory with a grass understory. Three primary scene components were selected for this site: 1) sunlit canopy 2) sunlit understory, and 3) shadowed canopy and understory. The IH-1 site is also a lodgepole pine overstory but contains a more complex understory of rocks, soil and litter. Four primary scene components were selected for this site: 1) sunlit canopy, 2) sunlit soil/litter, 3) sunlit rocks, and 4) shadowed canopy and understory.

Following the determination of the primary scene components for each site, a mosaic of 8" X 8" black and white prints was constructed depicting a complete 150 foot (45.7m) transect for the M-3 and the IH-1 site. The photographs used to create the mosaics were obtained on a cloudy day to minimize shadowing. These mosaics plus uncut duplicate 8" X 8" prints were used as a reference to pinpoint scene locations of individual 70mm photographic negatives which were used in the analysis procedure.

Proportions of the primary scene components for each scene were determined by video density slicing the black and white negatives using the Spatial Data Systems (Tech. Manual, Model 401/703) data color image enhancement system. This system allows video display of the black and white negatives for each scene. The unit can identify, color code and compute the proportion of the total scene displayed for up to 32 separate density intervals.

The density slicing procedure began with the selection and identification of a negative for a particular scene using the photo mosaic and enlarged prints for reference. A mask which defined the precise radiometer field of view (Section 3.2) was positioned over the negative. This mask allowed only the portion of the scene which was viewed by the

radiometer to be displayed on the color image enhancement system. The total density range of the masked scene was determined on the machine to fix the upper and lower bounds so that densities outside of the desired range would not be considered. Primary scene components were coded on the video image based on their density interval and further defined using the unshadowed enlarged prints of the same area. The system was then used as an aid in computing the proportion of each of the components when coding was completed (Figure 16, A & B). This procedure was repeated for each of the negatives that were evaluated for proportions of primary scene components.

Coding of proportions for scenes from the M-3 site produced the following results. Shadow areas coded well because of the density contrast with the remainder of the scene. Understory and canopy components were somewhat more difficult to code requiring operator estimation of proportions in conjunction with coding for some scenes due to overlap in densities for the two components. Coding of proportions for scenes from the IH-1 site was more difficult. The canopy and the two understory components were quite different spectrally, so coding of the canopy components posed no real difficulty. The two understory components separated well, also because of the spectral difference between the rocks and the soil/litter components. The problem was in coding the shadowed regions because of the large spectral variation in the understory. This resulted in a varied range of densities within the shadowed areas which could not reliably be coded as separate components.

In order to estimate the potential for error in this method, three operators were used in determining proportions. Replications of measurements were repeated by a single operator and also by using different

Fig. 16 A A photographic record of composite forest scene (Pinus contorta). Relative proportions are sunlit trees, 40%; sunlit understory 6%, shadows, 54%.

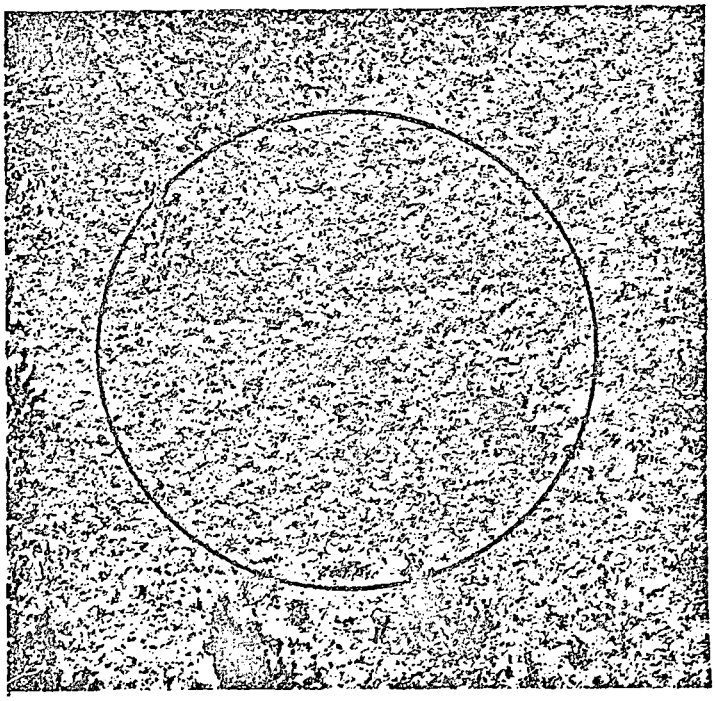

Fig. 16 B Photographic record of composite understory scene. Relative proportions are sunlit trees, 0%; sunlit understory 98%; shadows, 2%.

operators. This produced an average variance in proportion estimates of less than 5% for scene from the M-3 site and less than 10% for scenes from the IH-1 site.

Once proportion estimates were completed for all of the desired scenes, the values were combined with the corresponding spectral reflectance values for use in further analysis. A data listing containing proportions and spectral reflectance values for each scene analyzed, is presented in Appendix A. Table 3 summarizes the number of observations obtained by date and site.

TABLE 3. Summary of observations

Site	Date	# of Observations
M-3	8/10/76	8
M-3	8/12/76	24
M-3	8/21/76	31
M-3	9/17/76	20
IH-1	9/13/76	24

5.0 ANALYSIS

Data analysis to determine the relationship between proportions of scene components and spectral reflectance from the scene encompassed several stages.

Initially, various scatter plots of reflectance data and scene component proportions were made to evaluate trends and relationships within the data. Zenith sun angles were computed for all data points. Eigenvalues and eigenvectors were calculated for the data for the M-3 and IH-1 sites. These were used to compute and plot the ellipses of concentration for the observations at each of the sites. A regression model was developed on data from the M-3 and the IH-1 sites. The linear regression model uses proportions of scene components and zenith sun angle as potential independent variables to predict each of the six spectral reflectance bands. A test of the model was employed using regression equations developed on randomly selected points from approximately one half of all of the analyzed August data obtained over the M-3 site. These equations developed on one half of the August data sets were applied to the remaining half of the data sets to evaluate the accuracy of the regression model. An additional analysis of component proportion coefficients was conducted in an attempt to evaluate the theory that each of these coefficients represent that particular component's reflectance.

5.1 Scatter Plot Analysis

Three types of scatter plots were constructed using the M-3 and the IH-1 reflectance data. 1) Plots of component proportions versus scene spectral reflectance for .675μm and .96μm bands, 2) plots of location

along the transect versus scene spectral reflectance in the .675μm and .96μm bands, and 3) plots of reflectance at 0.675μm versus reflectance at 0.96μm. Analysis of scatter plots of all combinations of spectral bands indicated that reflectance values at .675μm plotted against reflectance values at .96μm provided the best dispersion of the data cluster. This dispersion facilitates analysis of subtle variations in the data. These two bands, .675μm, and .96μm tend to be the most responsive to variations in vegetation caused by both proportion and phenological changes. The .675μm wavelength is the chlorophyll absorption band and is sensitive to changes in amount of chlorophyll as a function of varied densities of vegetation types or phenological changes in the vegetation. The .96μm wavelength is in the near infrared range which is sensitive to vegetative vigor especially as a function of plant water.

Six plots displaying component proportions versus spectral reflectance for the M-3 site are presented in Figure 17 (A-F). Eight plots displaying component proportions versus spectral reflectance for the IH-1 site are presented in Figure 18 (A-H). Each of the two sets of plots was interpreted as a group to help evaluate the interaction between the proportions and scene spectral reflectance.

Plots depicting scene spectral reflectance as a function of transect position for the M-3 site and the IH-1 site are displayed in Figure 19 (A and B) and Figure 20 (A and B) respectively. Symbols used for data points represent individual sets of data collected as labeled for each figure. An individual set of data, in this case refers to one group of measurements taken consecutively at intervals along the transect. This type of plot provides an indication of the signature of the scene

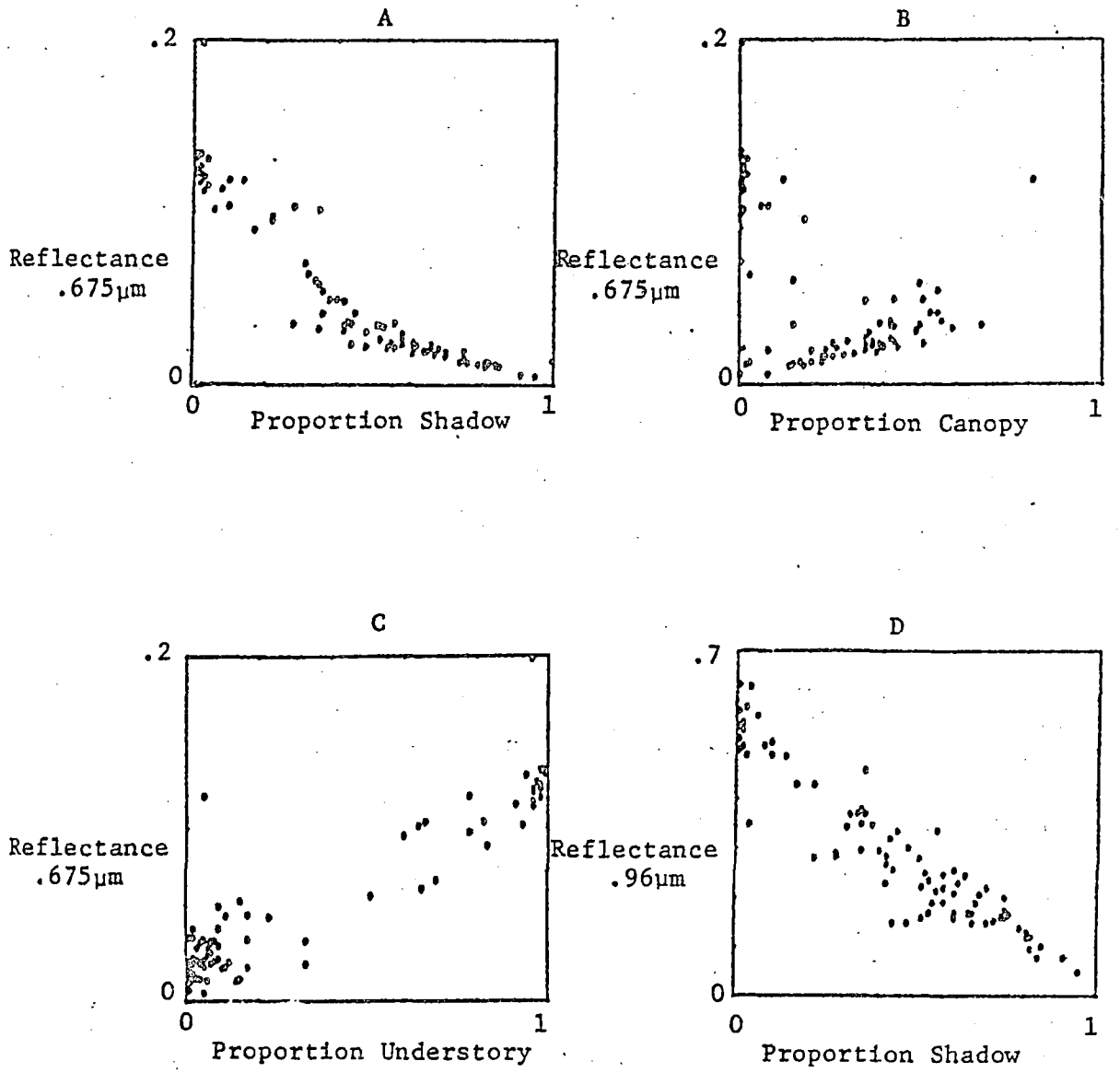

FIGURE 17 (A-D) M-3 Site
Proportion of scene components versus reflectance at .675μm and .96μm bands

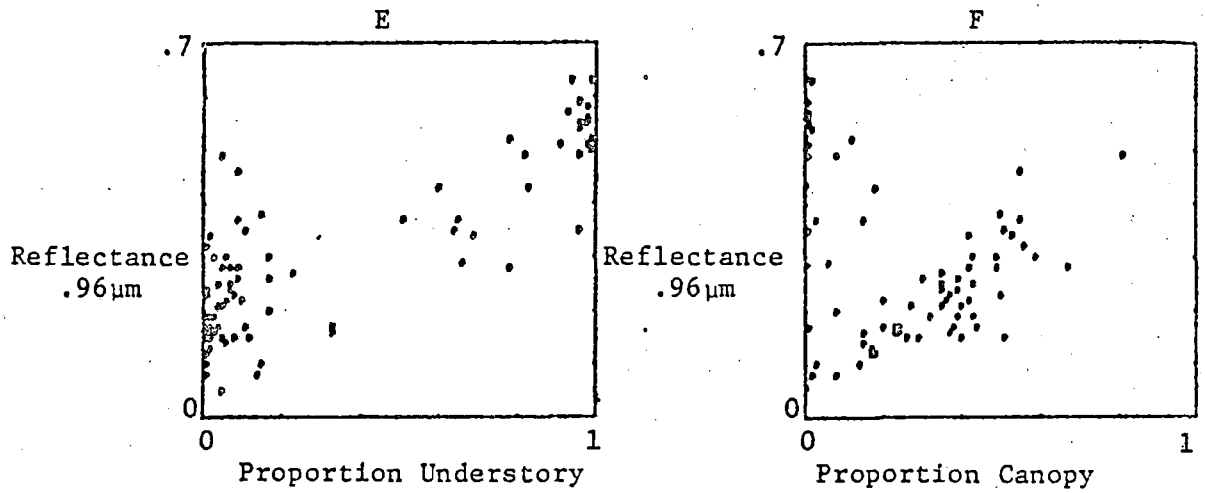
E
.7
Reflectance
.96μm
0
0
1
Proportion Understory
F
.7
Reflectance
.96μm
0
0
1
Proportion Canopy

FIGURE 17. (E-F)

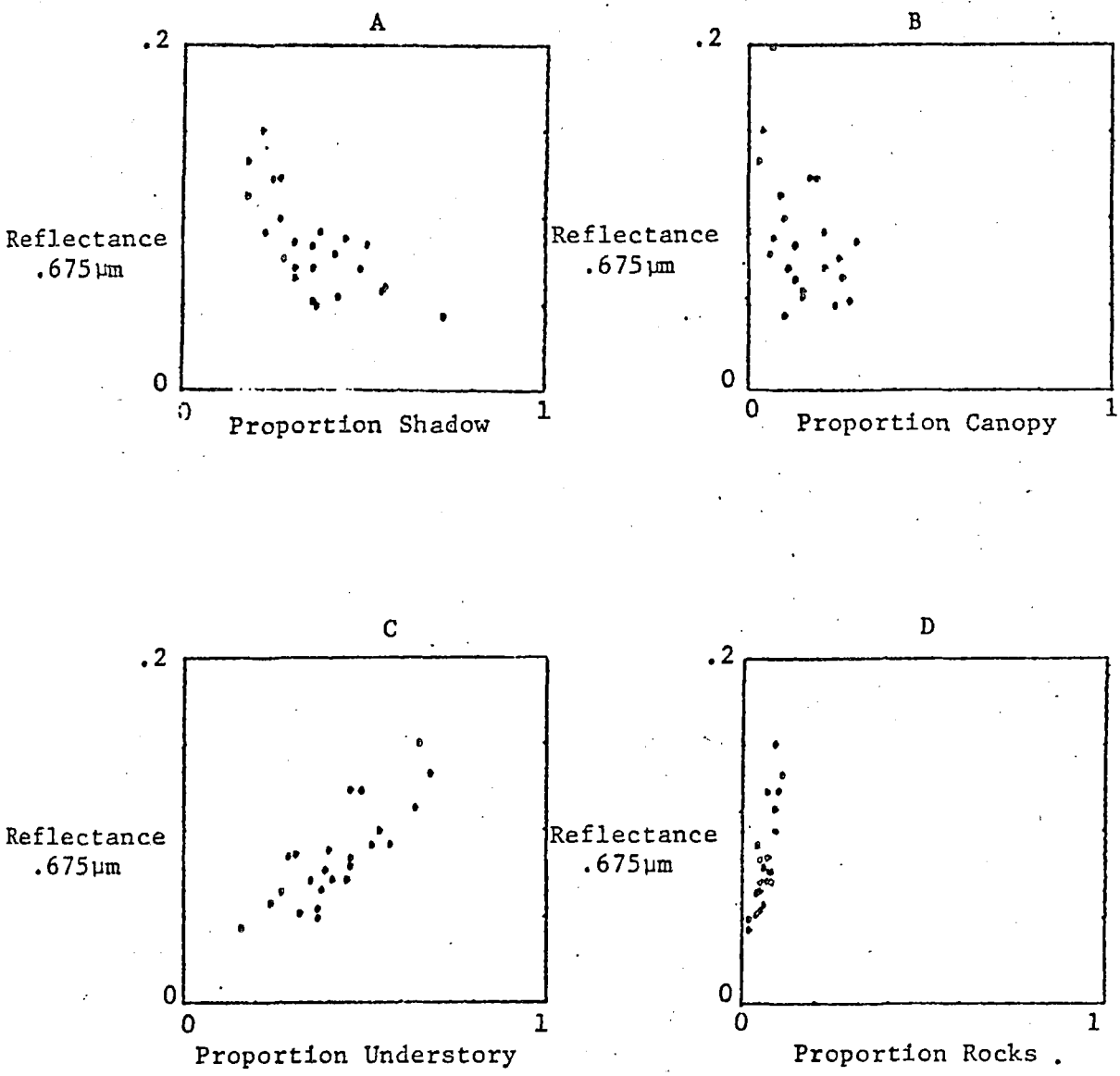

FIGURE 18. (A-D) IH-1 Site Proportion of scene components versus reflectance at .675µm and .96µm bands

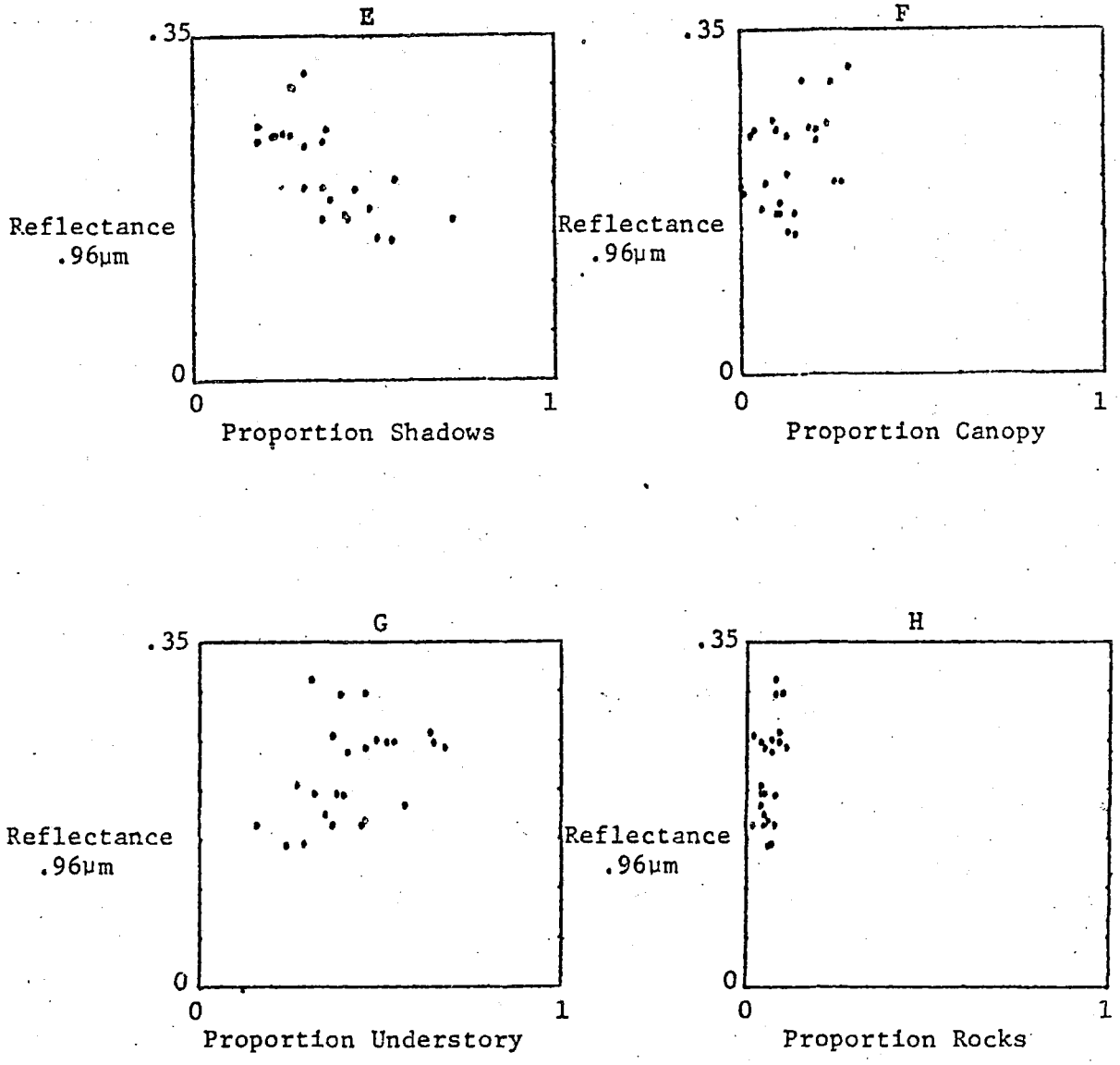
E
.35
Reflectance
.96µm
0
0
1
Proportion Shadows
F
.35
Reflectance
.96µm
0
0
1
Proportion Canopy
G
.35
Reflectance
.96µm
0
0
1
Proportion Understory
H
.35
Reflectance
.96µm
0
0
1
Proportion Rocks

FIGURE 18. (E-H)

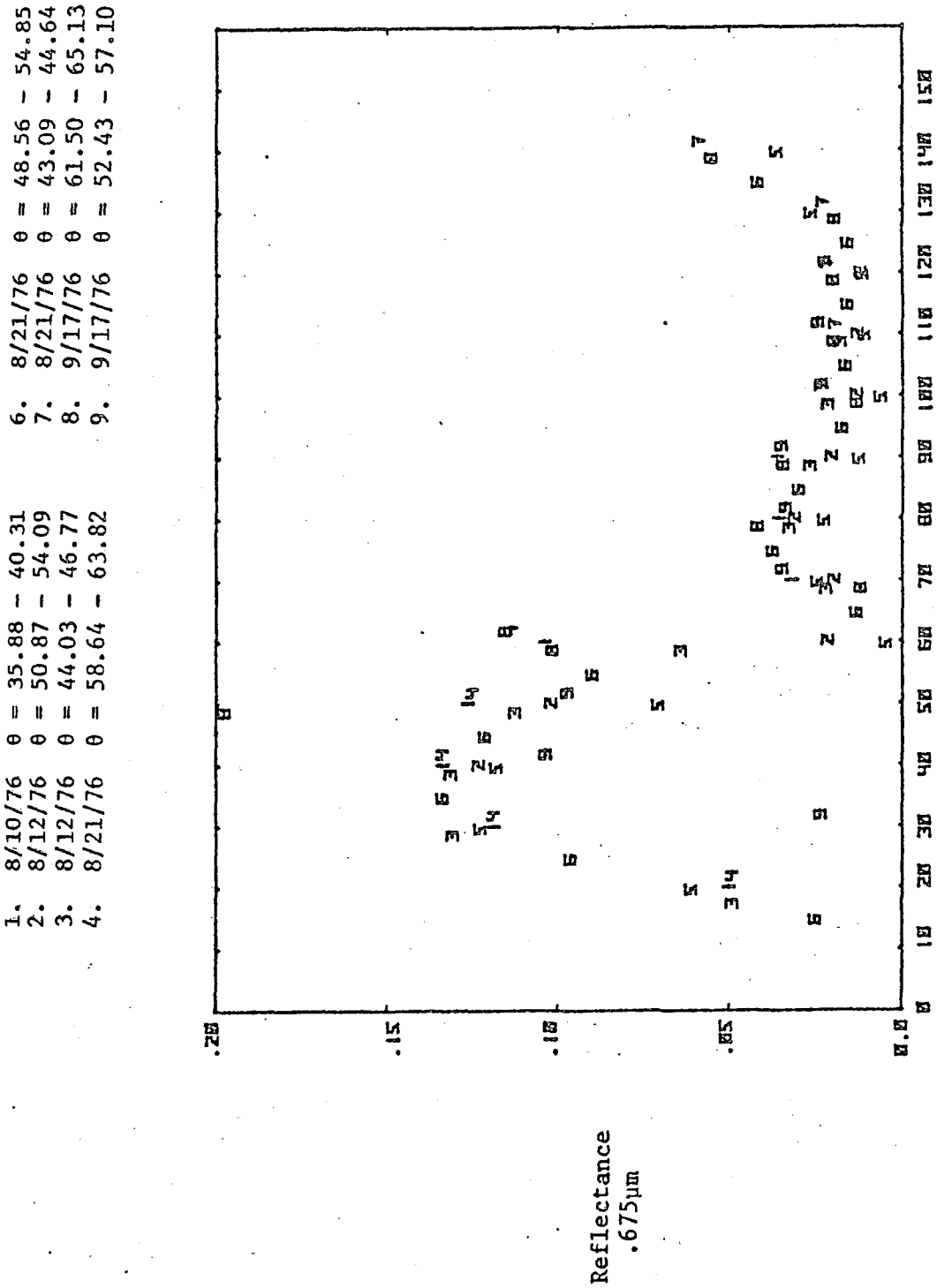

FIGURE 19 A. M-3 Transect Position versus reflectance at .675µm band

1.	8/10/76	θ = 35.88 - 40.31	6.	8/21/76	θ = 48.56 - 54.85
2.	8/12/76	θ = 50.87 - 54.09	7.	8/21/76	θ = 43.09 - 44.64
3.	8/12/76	θ = 44.03 - 46.77	8.	9/17/76	θ = 61.50 - 65.13
4.	8/12/76	θ = 34.19 - 35.13	9.	9/17/76	θ = 52.43 - 59.10
5.	8/21/76	θ = 58.64 - 63.82			

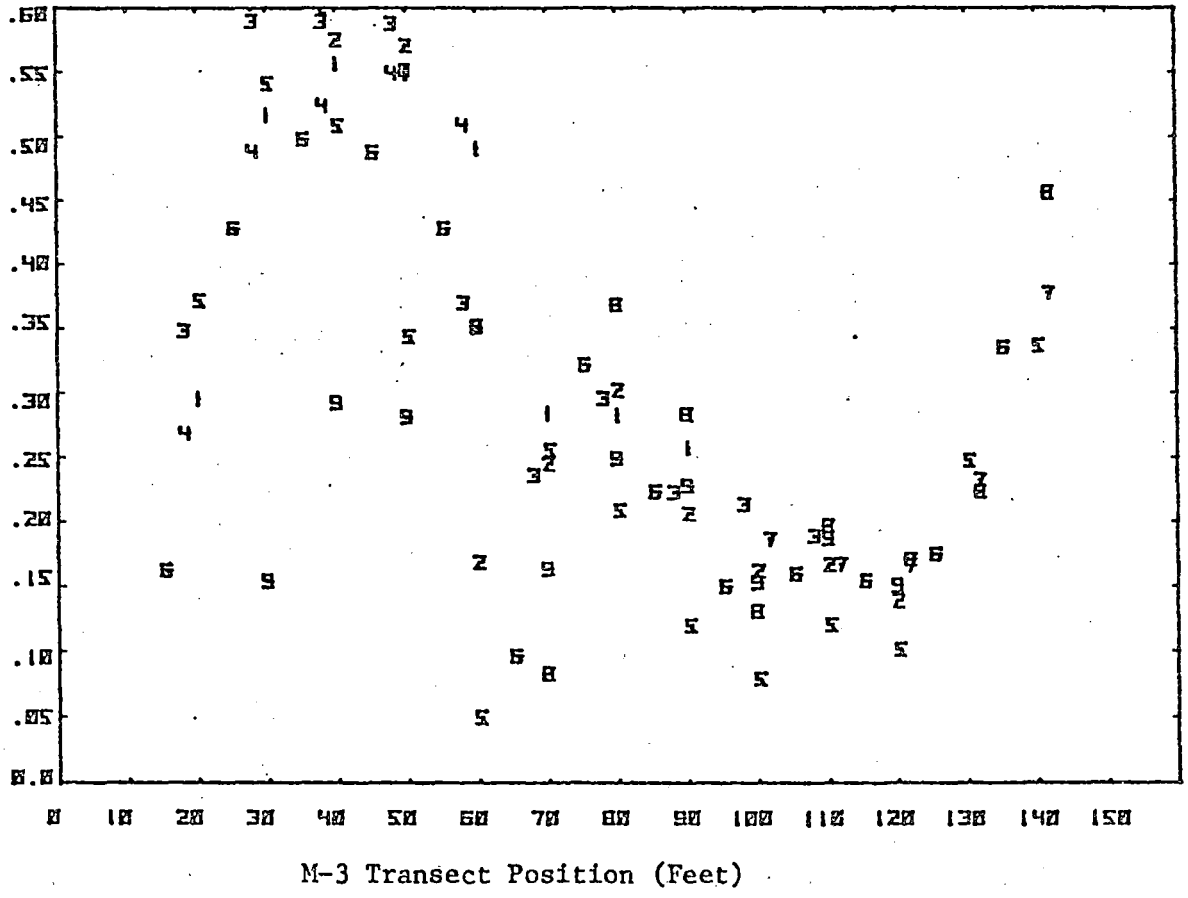

Figure 19 B. Transect position versus reflectance at .96μm band

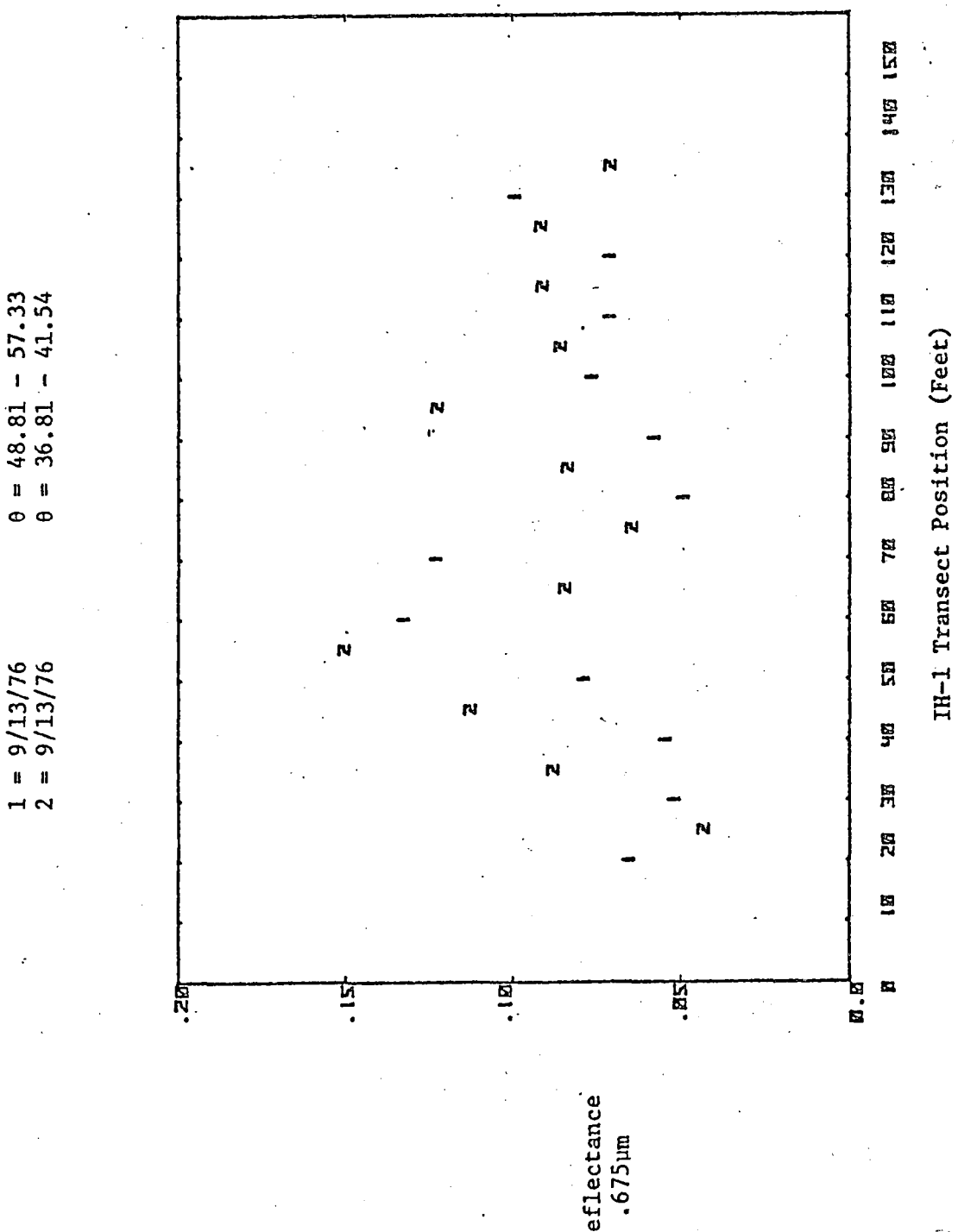

FIGURE 20 A. IH-1 Transect position versus reflectance at .675µm band

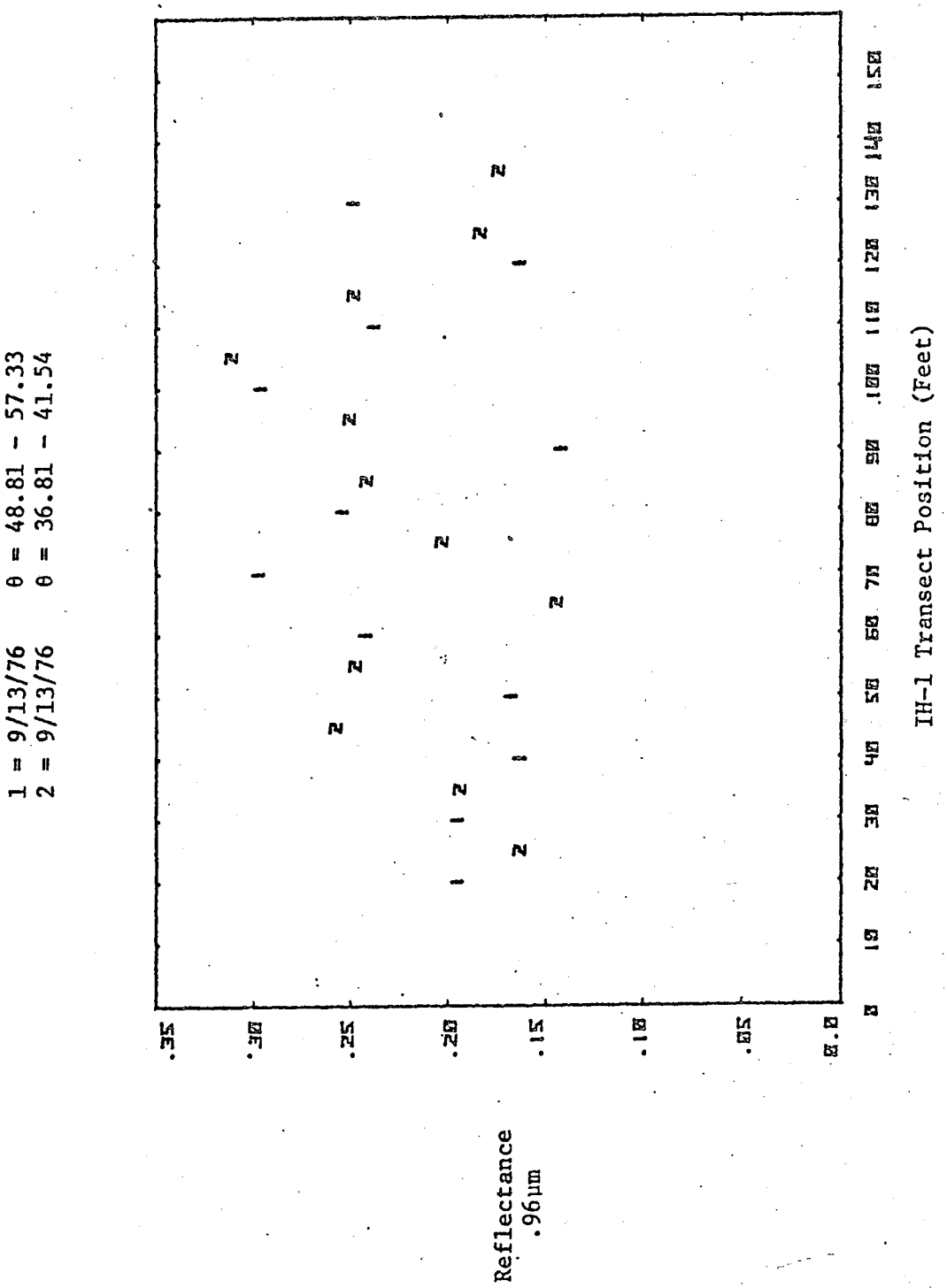

FIGURE 20 B. IH-1 Transect position versus reflectance at .96µm band

along the transect. These plots also allow the examination of data spread for a particular point along the transect.

Plots displaying the scene spectral response at .675μm versus the scene spectral response at .96μm for the data collected at the M-3 site and the IH-1 site are presented in Figure 21, and Figure 22 respectively. The symbols represent different dates of data acquisition as labelled in the figures. This procedure was used to determine if the spectral trend of the data cluster changed with the date of acquisition due to phenology changes in the vegetation.

An additional plot displaying scene spectral response at .675μm versus the scene spectral response at .96μm was constructed for the M-3 data. This plot separated data points into categories of primarily understory and primarily forest (Figure 23). Since the physical structure of the scene along the M-3 transect consists basically of either a relatively dense canopy or an open meadow area, it was thought that the spectral characteristics of these two scene types would be quite different. A decision was made to separate data into two categories representing these two general scene types. Criteria for defining understory points (meadow area) required that proportion of understory be greater than 40% and in addition that the proportion of canopy be less that 10%. The criteria for the determination of forest category data points required that the proportion of the canopy be greater than 30% with the proportion of the understory being at 20% or less. These criteria were determined by analysis of all the data, considering position along the transect in addition to the relationship between proportions. Percentage criteria for the forest category are less stringent than the understory class because of the high proportion

A = 8/10/76 data
B = 8/21/76 data
M = 8/12/76 data
G = 9/17/76 data

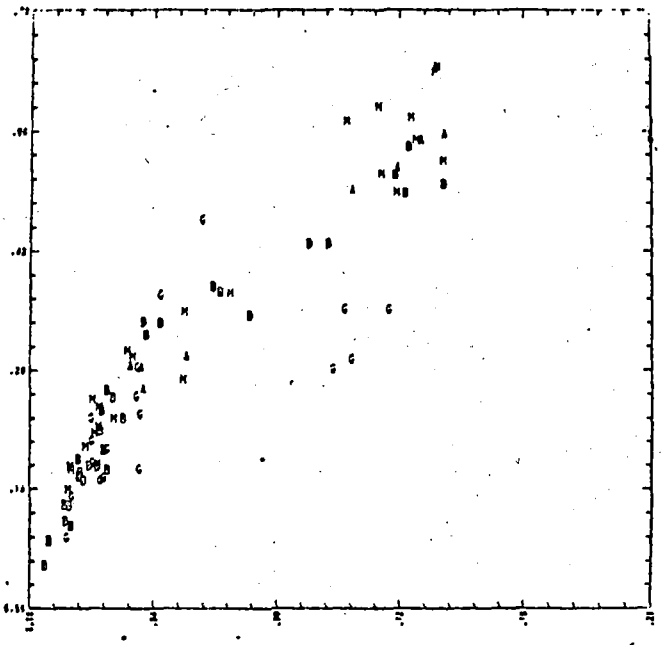

Reflectance .96μm

Reflectance .675μm

FIGURE 21. M-3 site .675μm band reflectance versus .96μm band reflectance

H = 9/13/76 data

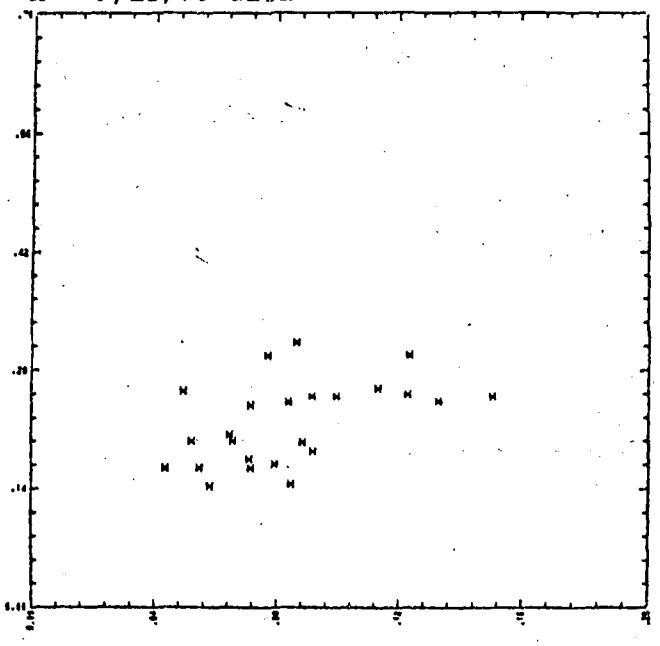

Reflectance .96μm

Reflectance .675μm

FIGURE 22. IH-1 site .675μm band reflectance versus .96μm band reflectance

C = Canopy U = Understory

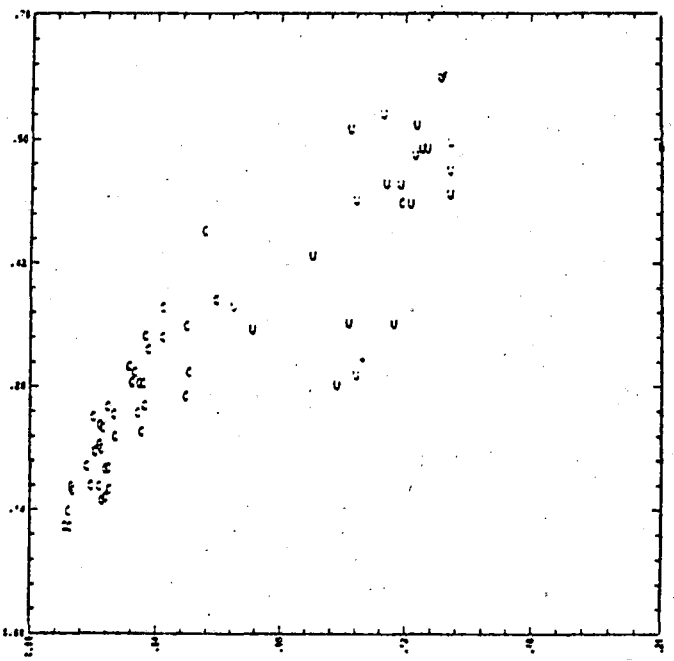

Reflectance .96 m

Reflectance .675 m

FIGURE 23. M-3 site .675 m band reflectance versus .96 m band reflectance

Canopy and Understory Categories

of shadows present in the forested areas. Points that did not meet the criteria for either class were not considered in this specific analysis. This resulted in the removal of 20 data points. This latter plot allows examination of the spectral characteristics of the understory and canopy components relative to one another.

5.2 Sun Angle Calculation

Studies by Oliver and Smith (1974) and Smith and Oliver (1974), indicate sun angle induced changes in scene reflectance for short grass canopies. Sun angle and spatial distribution of trees within a forest scene appear directly related to the proportion of shadows within the scene. Based on studies by other investigators and evaluation of data collected for this experiment, it was decided that sun angle might be a potentially important variable to include in a model describing the relationship between scene components and scene spectral response. Slope and aspect are considerations in the computation of sun angle relative to the scene. However, slope on both the M-3 and the IH-1 site is small enough that its affect was considered minimal for these analyses and was not computed. The solar zenith angle computation program requires the input of the following information 1) latitude of the site, 2) declination based on the date, 3) the equation of time which is a function of the declination, and 4) the local time of day and whether it is standard or daylight savings time. Output from the computation program includes latitude, date, declination, equation of time, whether time is standard or daylight savings and the local time and its associated solar zenith angle. The program listing is contained in Appendix B. The computational formula for the computation of the

solar zenith angle is:

$$\text{Cos}\theta_s = \text{Sin}_\delta \text{Sin L} + \text{Cos}_\delta \text{Cos L Cos h}$$

where

θ_s = Solar zenith angle

δ = declination

L - latitude

h = solar hour angle

The value of h in degrees is given by the equation:

$$h = 15.(t-N)$$

where

t = local standard time

N = 12.083 + equation of time

Computed solar zenith angles are presented along with proportion and reflectance data in Appendix A.

5.3 Eigenvalue, Eigenvector and Ellipse of Concentration Determinations

Eigenvalues and eigenvectors were computed for both the IH-1 data and the M-3 data. In addition eigenvalues and eigenvectors were computed for M-3 data which was separated into forest and understory categories. This following discussion of eigenvalues and eigenvectors represents a two dimensional case for ease of description. Eigenvalues and eigenvectors are used to define the ellipse of concentration for the data set being considered. The eigenvalues represent the magnitudes or lengths of the major and minor axis of the ellipse. The eigenvectors describe the orientation of the ellipse relative to the axis of the coordinate system, in this case, the original spectral bounds. Eigenvalues and eigenvectors are not limited to a two dimensional analysis. They may

be considered in n dimensions thus producing a hyperellipsoid in n dimensional space. The ellipse of concentration can be interpreted as the boundary around the data cluster which contains the data that is within one standard deviation of the mean of the cluster. In the two dimensional case it describes the covariance or joint variation of two variables about their common mean. A general description of eigenvalues and eigenvectors is contained in Davis (1973). The discussion by Davis includes computational procedures in addition to clear concise explanation of eigenvalues and eigenvectors.

Eigenvalues and eigenvectors and the resulting ellipses of concentration for .675μm and .96μm reflectance data from both the M-3 and the IH-1 sites are presented in Figure 24. This plot was presented to display the spectral separation and distribution of data collected over the two sites. Figure 25 displays the ellipses of concentration of M-3 data separated out as understory and forest in addition to the ellipse representing all of the M-3 data. Forest and understory data used in computation of the eigenvalues and eigenvectors were the same as those selected for the scatter plots as discussed in Section 5.1. The plot of the ellipses of concentrations for the forest and understory groups provides a means of evaluation of the spectral separation between them and also their relationship to the ellipse of concentration for the total unseparated M-3 data.

Eigenvalues and eigenvectors were computed using a CDC system subroutine entitled "EIGRS" (IMSL, 1975). This subroutine is implemented on the Colorado State University CDC 6400 computer. In the case of the 2 dimensional analysis employed in this study the input to the subroutine is the 2 x 2 covariance matrix associated with the .675 and .96μm bands.

Site	Mean		Eigenvalues		Major Axis Eigenvectors	
	.675	.96	λ1	λ2	Δx	Δy
M-3	.05501	.30189	.00047	.02553	.24709	.96899
IH-1	.08435	.21796	.00038	.00262	.52573	.85065

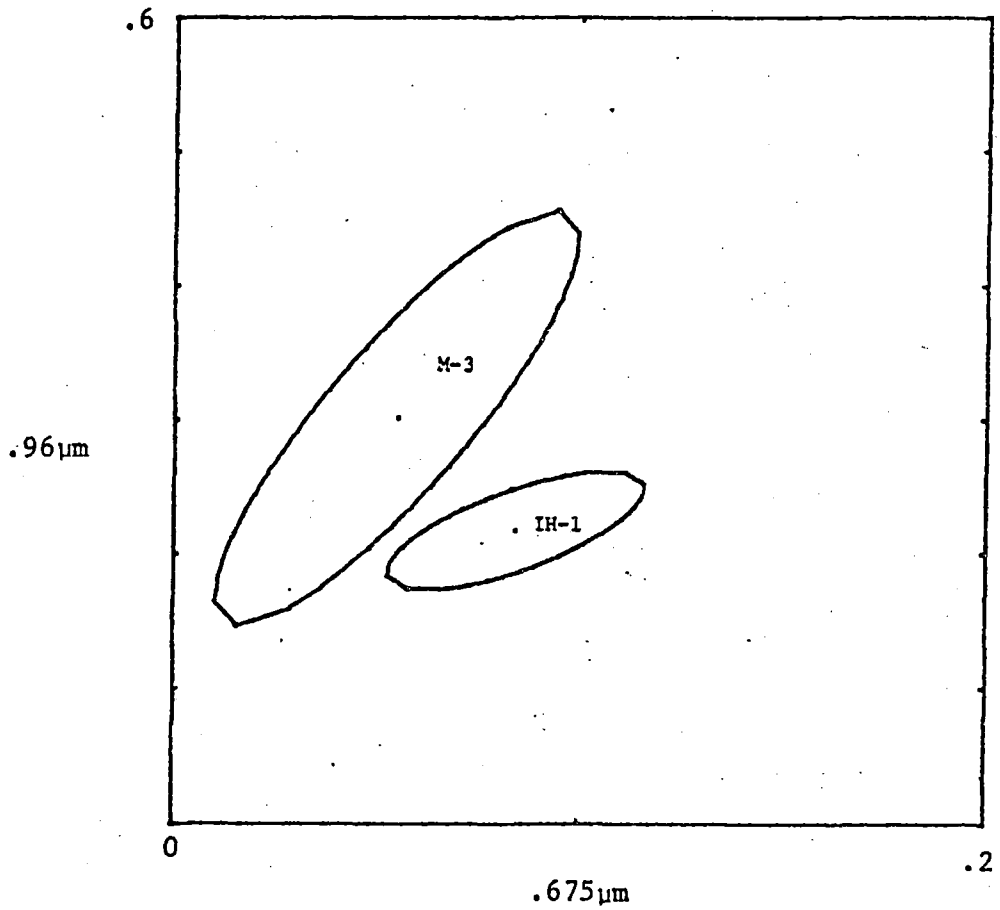

FIGURE 24. Ellipse's of Concentration (M-3 and IH-1)

Site	Mean		Eigenvalue		Major Axis Eigenvector	
	.675	.96	λ1	λ2	Δx	Δx
M-3	.05501	.30189	.00047	.02553	.24709	.96899
Canopy	.03139	.24592	.00014	.00714	.1390	.9903
Under-Story	.11672	.48630	.00035	.01135	.1735	.9848

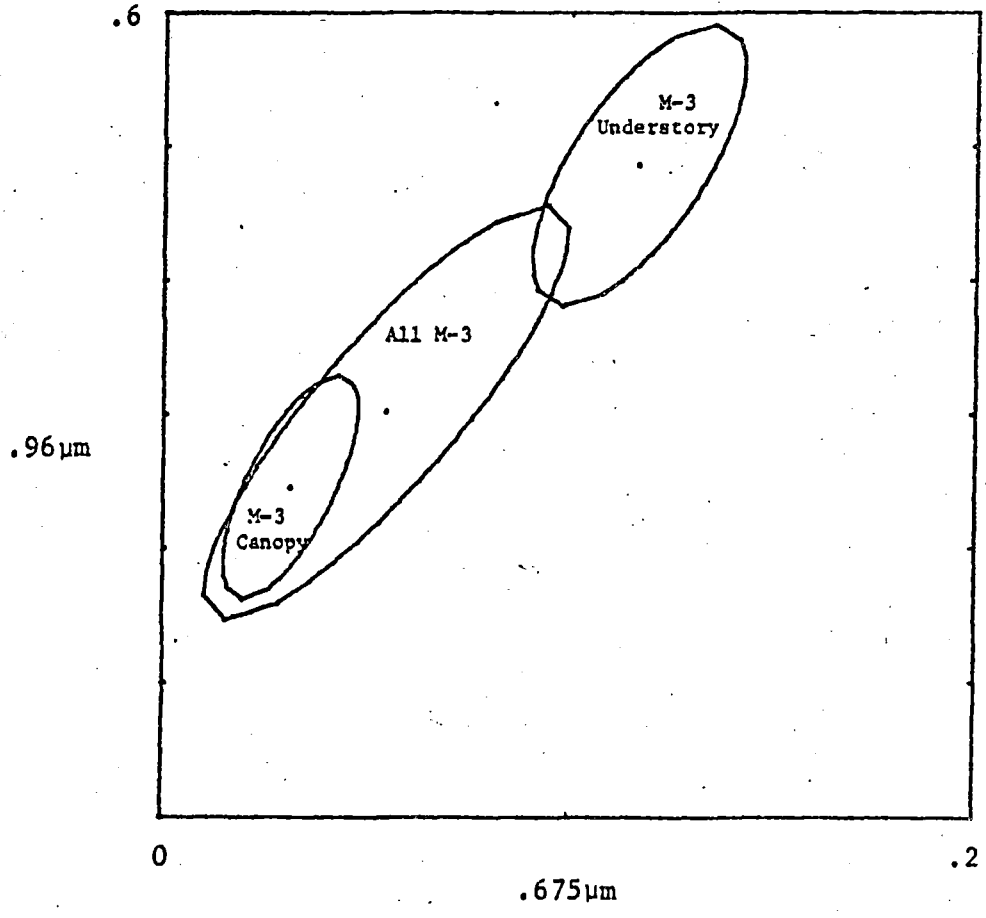

FIGURE 25. M-3 Ellipse's of Concentrations (Canopy, Understory, All M-3)

Output from the program includes two eigenvalues and a two x two matrix of eigenvectors for each covariance matrix that is input.

A listing of the program utilized to plot ellipses of concentration is contained in Appendix B.

5.4 Linear Regression Model

A linear regression model was developed using scene component proportions and zenith sun angle as the independent variables, and each of the six spectral bands reflectance values as the dependent variables.

$$\hat{y}_m = b_0 + b_1X_1 + b_2X_2 \ldots + b_nX_n + \varepsilon$$

where

$\hat{y}_m$ = reflectance values for a single spectral band, m

b_0 = y intercept of the regression line

b_n = the slope coefficient for variable X_n

X_n = scene component proportion or sun angle

ε = error term

In matrix notation the equation is of the form -

$$Y = XB + \varepsilon$$

Y = vector of reflectance values

X = matrix of independent variables (Proportions and sun angle)

B = vector of parameters to be estimated

ε = vector of error terms

Draper and Smith (1966) provides a comprehensive, detailed description of Regression analysis techniques.

A stepwise regression technique was applied to the data because of its ability to select the best set of independent variables for each of the regression equations. This type of approach selects the independent

variable most highly correlated with y for the first step of the regression. In subsequent regression steps, this technique selects from the remaining variables the one with the highest correlation with y.. However, it also re-examines those variables already incorporated in the model to see if they still contribute significantly to the regression after the addition of a new variable. A variable which may have been the best single variable to enter at an early stage may, at a later stage, be superfluous because of the relationships between it and other variables now in the regression. A partial F criteria is used to determine whether a variable will be entered or removed from the regression at each step. The following discussion from Davis (1973) describes the F distribution and its application. Tests to determine equality of variances are based on a probability distribution called the F distribution. This is the theoretical distribution of values that would be expected by randomly sampling from a normal population and calculating, for all possible pairs of sample variances, the ratios

$$F = \frac{s_1^2}{s_2^2} .$$

It seems reasonable that the sample variances will range more from trial to trial if the number of observations used in this calculation is small. Therefore, the shape of the F distribution could be expected to change with changes in sample size. The F distribution is dependent upon two values of degrees of freedom, one associated with each variance in the ratio. Degrees of freedom are simply defined as the number of observations in a sample, minus the number of parameters estimated from the sample. Because the F distribution describes the probabilities of obtaining specified ratios of sample variances drawn from the same population, it

can be used to test the equality of variances which were obtained in statistical sampling. We may hypothesize that two samples are drawn from populations having equal variances. After computing the F ratio, we then can ascertain the probability of obtaining, by chance, that specific value from two samples from one normal population. If it is unlikely that such a ratio could be obtained, we regard this as indicating that the samples came from different populations having different variances.

The F test as applied to the regression situation tests to see if there is a significant difference between the variance about the regression line and the variance in observations. If the calculated F ratio exceeds the Table or "critical" F value selected for a certain level of significance, then the hypothesis that the variance of the observations is equal to the variance about the regression line is rejected. An α value is generally used to represent the level of significance. A value of $\alpha = .05$, refers to the 5% level of significance. This means that when the F value calculated exceeds the critical F value for $\alpha = .05$, we can reject the hypothesis that the variance of the observations is the same as the variance about the regression line with a risk of less than 5% of being wrong. This indicates that there is a significant amount of variance in the data which is accounted for by the regression. The partial F test used in stepwise regression is essentially the same as the F test just described. In stepwise regression, however, the partial F value for each variable in the regression at any stage of calculation is evaluated and compared with a preselected percentage point of the appropriate F distribution. This provides a judgment on the contribution made by each variable as though it had been the most recent variable

entered, irrespective of its actual point of entry into the model. The $\alpha = .05$ F criteria were applied to this study in the stepwise regression procedure for determination of variables to be included or removed from the equations. A detailed description of stepwise regression procedures and F tests, including formulas used for computations, is presented in Draper and Smith, 1966.

Regression analysis of the M-3 data involved the following approaches. Independent variables available for use in the model included zenith sun angle, proportion of shadow, proportion of sunlit canopy and proportion of sunlit understory. Regression equations were developed on data for each of the following dates of acquisition, August 10, 12, 21 and September 17, 1976. Based on results from regressions done on data for individual dates, it was decided to combine all of the August data for analysis. After combining the August data into one group, one half of the data was selected to develop the regression equations. The resulting regression equations were then applied to the remaining August data in an attempt to evaluate the prediction accuracy of the regression. A listing of the computer program utilized in the evaluation procedure and an explanation of its computational methods are included in Appendix B. Regression analysis was also used for data from the IH-1 site to investigate its utility in a more complex scene. Data for this analysis was collected on one date, August 13, 1976 so only one set of equations was developed. Independent variables available for selection in the model included zenith sun angle, proportion of shadow, proportion of canopy, proportion of understory and proportion of rocks.

Shadows are a principal component in all of the proportions estimates. However the b_n term applied to the shadow component is somewhat nebulous. Based on this factor, a decision was made to delete shadows as a potential independent variable in the regression model. This has the effect of combining the b_n term for the shadow component with the intercept term in the regression equation. This is true because the proportions of scene component must sum to one. In the use of three scene components, this allows the regression equation to be expressed as a function of two scene components with the third component represented in the intercept term.

$$\hat{y} = b_0 + b_1X_1 + b_2X_2 + b_3X_3 + \varepsilon$$

by representing X_3 as a function of X_1 and X_2 then

$$\hat{y} = b_0 + b_1X_1 + b_2X_2 + b_3(1-(X_1 + X_2)) + \varepsilon$$

combining terms

$$\hat{y} = (b_0 + b_3) + (b_1 - b_3)X_1 + (b_2 - b_3)X_2 + \varepsilon$$

$$\hat{y} = b_0^1 + b_.^1X_1 + b_2^1X_2 + \varepsilon$$

The same condition is true for expressing four original scene components as a function of three of them. This combining procedure was utilized in all of the regression analyses for both the M-3 and the IH-1 data.

Using the model

$$y_m = b_0 + b_1X_1 + \ldots b_nX_n + \varepsilon$$

when X_n equals a given proportion of a scene component, one interpretation is that the b_n term is an estimate of the reflectance of that component, providing that the proportions sum to one (Horwitz et al., 1971; and Pace and Detchmendy, 1972). This situation requires that only scene components can be included in the regression equation as independent

variables. Further, all scene components must be represented in the equation. In cases where all of the scene component variables, other than shadows, were utilized in the regression equation, a plot was constructed representing the b_n terms for each component. If these terms do represent the reflectances of the companion scene components, then the plots of the b_n values versus wavelength should describe a curve representing the signature of that component. Since only scene components can be included as independent variables for investigation of this hypothesis, sun angle was not included as a potential independent variable for this specific analysis. Canopy and understory coefficient values and their respective wavelengths for regression equations developed on August 12, 21 and September 17 data are presented in Table 4. Plots of understory and canopy coefficient versus wavelength for each data group is presented in Figures 26 and 27 respectively. Analysis of coefficients as applied to the M-3 data was not done on IH-1 data because not all scene components were significant variables in certain equations.

TABLE 4. Coefficients for proportions of canopy and understory (M-3) data

Data	Component	Coefficients of Variables: Wavelength					
		.4600μm	.5145μm	.5500μm	.6750μm	.8000μm	.9600μm
8/12/76	Understory	.073	.100	.144	.156	.458	.571
	Canopy	.066	.090	.129	.135	.431	.508
8/21/76	Understory	.054	.078	.116	.128	.470	.514
	Canopy	.037	.061	.103	.076	.560	.518
9/17/76	Understory	.072	.093	.110	.172	.317	.410
	Canopy	.036	.052	.088	.080	.434	.436
½ All August Data	Understory	.065	.091	.133	.142	.463	.551
	Canopy	.052	.076	.115	.109	.455	.509

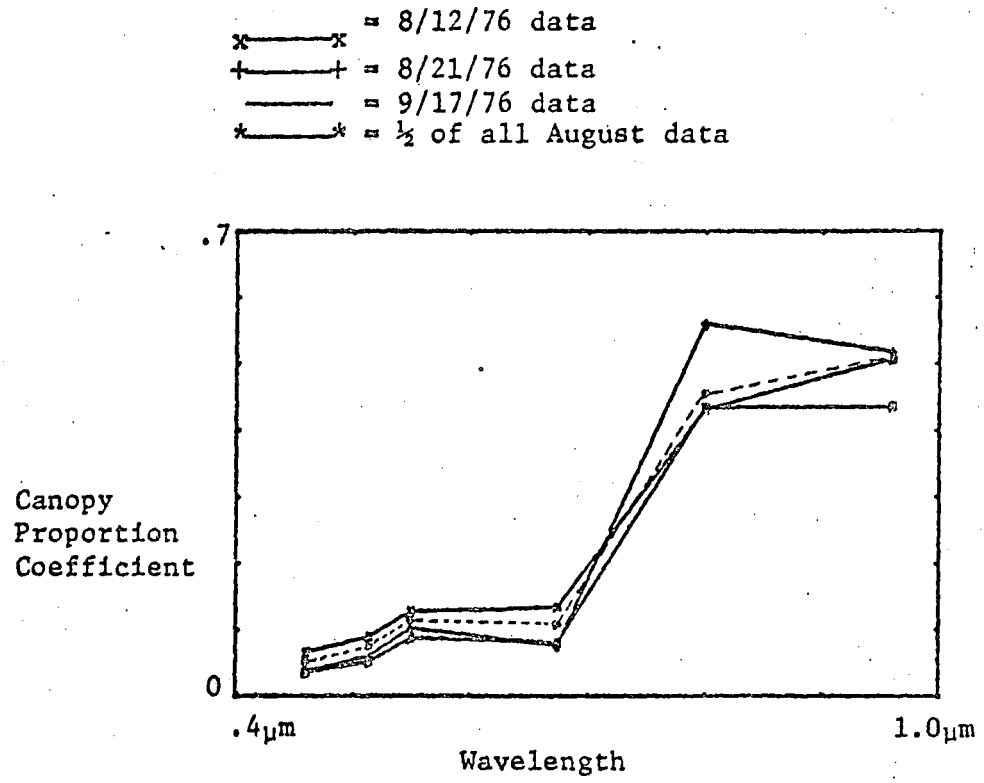

FIGURE 27. Wavelength versus canopy proportion coefficients (4 data groups)

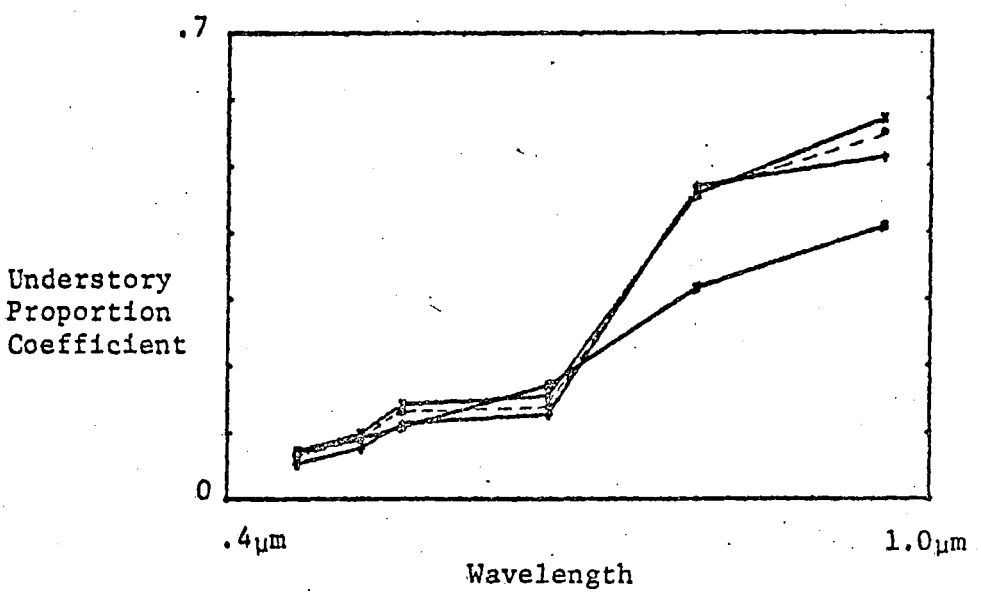

FIGURE 26. Wavelength versus understory proportion coefficients (4 data groups)

6.0 RESULTS AND DISCUSSION

Results from the analysis are presented by the same categories as discussed in Chapter 5. Categories for analysis included 1) scatter plot analysis of data 2) sun angle calculation 3) eigenvalue, eigenvector and ellipse of concentration determinations, and 4) linear regression model development and testing.

6.1 Scatter Plot Analysis

Plots of component proportions versus reflectance values at .675μm and .96μm for M-3 site data (Figure 17 A-F) graphically display the general relationships between individual scene components and reflectance. Shadows exhibit a relatively strong linear decreasing trend with increased proportion for both wavelengths. This is expected because of reduced scene radiance with increased amounts of shadowing. Reflectance values tend to exhibit a wider spread for lower proportions of understory with lesser data spread for very high proportions. The wide spread of reflectance values for low proportions of understory is a function of varying proportions of shadows and canopy. Higher reflectances for low understory proportions are the result of higher canopy proportions relative to the shadowing and vice versa for lower reflectances at this range. Reflectance values compared with proportions of canopy follow the same general trend as with the understory component. However, the reflectance values exhibit a wider spread for low canopy proportions than they do for low understory proportions. This is because the central meadow opening may have very high reflectance values with little or no canopy, while some shaded meadow areas adjacent to the overstory will have very low reflectance. Canopy proportions fall

in the range of 0-60% because significant shadowed areas are always present in the overstory due to the structure of the trees. In general, the trends discussed here are more pronounced in the .96μm band than the .675μm band.

Figure 18 A-H indicated proportions of each of the four scene components measured at IH-1 versus the scene reflectance for the .675μm and .96μm bands respectively. Evaluation of these plots is more difficult than for the M-3 data because there is less variation in proportions of components and the component relationships are more complex. There is a general decreasing trend in reflectance for both wavelengths as the proportion of shadows increases. This trend is the same as that exhibited for the M-3 site although it is less pronounced. There is an increase in reflectance in the .675μm band as the proportion of understory increases. Understory on this site is primarily bare soil and litter, which produces higher reflectance values in the .675μm band and lower reflectance values in the .96μm when compared to the M-3 site. As canopy proportions increase, there is a general decreasing trend in reflectance in the .675μm band. This is most likely a function of increased chlorophyll absorption and increased shadowing with an increase in the proportion of canopy. Reflectance in the .96μm band shows a slight increasing trend in reflectance for larger proportions of both canopy and understory components. It is difficult to note any defined reflectance trends associated with the proportions of rocks primarily because of the low proportions associated with this component.

The plots of reflectance in the .67μm and .96μm bands as a function of transect position for the M-3 and the IH-1 sites (Figures 19 and 20) display the general reflectance trends along the transect. As

discussed earlier each data collection transect is coded with a different symbol. This allows the comparison of data acquired at different dates and different sun angles to see if any discernible trends are present.

The M-3 site exhibits a more consistent trend of reflectance values along the transect than the IH-1 site. This is most likely caused by the large variation in proportions of the three scene components along the M-3 transect as compared to less variation in proportion and increased complexity of components at points along the IH-1 transect.

An examination of the general trend of reflectances along the M-3 transect highlights the meadow opening with generally high response in both bands in the region from 25 (7.6m) to 50 feet (15.2m). The wide spread of reflectance values in the area from 20 feet (6.1m) to 30 feel (9.1m) and 50 (15.2m) to 65 feet (19.8m) appears to be a function of shadowing from adjacent overstory. This is a result of varying sun angles and sun azimuth. The azimuth of the sun varies approximately 30^{o} for a given solar zenith angle on August 10, as compared to September 17. Examination of data from the .675μm band indicates that the spread of reflectances for a particular point along the transect may also be a function of sun angle. However, a detailed sun angle experiment is required to adequately describe this effect. Reflectances from the two September transects exhibit large deviations between one another and from the remainder of the data. Transect 8 exhibits high reflectance in the .675μm band in the area of the meadow opening. This is probably caused by browning of the meadow opening prior to the September 17 data collection period, as a result of

frost kill. This browning of understory was confined to the open meadow area of the M-3 transect. This browning would result in an increased reflectance in the chlorophyll absorption band. There appears to be no deviation of reflectance values over the meadow opening for the .96μm band. Transect 9 which was also measured on September 17 exhibits low reflectance values over the range of 30-50 feet (9.1-15.2 m) for both reflectance bands. These stations were the final three measurement points for data collection that day, and at that point the instrument battery power was at a minimum level. This may be the explanation for the sharply reduced reflectance values in this area of the transect when compared to values from the previous transect which were obtained less than one hour earlier.

Exact comparison of the two transects of data taken along the IH-1 site is difficult because one transect was measured at ten foot (3.0 m) intervals beginning at 20 feet (6.1 m) and the other was measured at 10 foot (3.0 m) intervals but beginning at 25 feet (7.6 m). The result is that no two stations encompass the same scene. As in the M-3 transect there is an indication that, in the .675μm reflectance band, the data spread at a given location along the transect may be a function of sun angle. This effect does not appear to be present in the .96μm band for either the M-3 or the IH-1 transect.

Figure 21 is a scatter plot of reflectance values at .675μm and .96μm for data from the M-3 site. Reflectance values are coded by date of acquisition. The wide range of data appears to be primarily a function of the large spread of component proportions. Scene characteristics vary from relatively dense forest to an open meadow. Several reflectance values from the September data set appear as

outliers below the main data cluster. Further investigation located these as points in the meadow opening. This reinforces the hypothesis formed about the September data in the discussion about reflectance trends displayed in Figures 19 and 21.

Based on the theory that the wide range of reflectances for the M-3 site is a function of diversity in component proportions, it was decided to create a plot separating the M-3 transect into canopy and understory categories. The criteria for this separation is presented in Section 5.1. Figure 23 depicts the reflectance values for the .675μm versus .96μm broken down into forest and understory categories. As expected, the two categories tend to separate out into two separate data clusters. As previously indicated for Figure 21, the September understory points appear as outliers below the main data cluster for the understory category.

Reflectance values at .675μm plotted versus reflectance values at .96μm for the IH-1 site are presented in Figure 22. The general data cluster is more compact than the data cluster for the M-3 site. This results from the fact that there is less spread in the proportions of each component. Reflectance spread along the .96μm axis for the IH-1 site is considerably less than that displayed for the M-3 site. This is most likely due to the lower proportions of canopy coupled with an understory component composed primarily of soil and litter which exhibits generally lower reflectance values for near infrared wavelengths.

6.2 Sun Angle Calculation

Solar zenith angles computed for all data observation times, over both the M-3 and the IH-1 sites, ranged from 35 degrees to 65 degrees.

Solar zenith angles less than 35° do not occur for two reasons. Data collection during the month of August was limited primarily to morning hours between 8:30 and 11:30 local daylight savings time. The sun reached its lowest zenith angle at about 13:00 local daylight savings time. Cloud formation, generally before noon, during the month of August restricted data acquisition past that time. Cloudy conditions abated somewhat during the September period, allowing data collection into the afternoon hours. However, by mid-September, the solar zenith angle at the sun's highest elevation is only about 35 degrees. The mean solar zenith angle for all data analyzed for both sites is approximately 50 degrees. This relatively low mean sun elevation (40 degrees above the horizon) results in considerable shadowing within the canopy and some adjacent areas.

6.3 Eigenvalue, Eigenvector, and Ellipse of Concentration Determination

Eigenvalues, eigenvectors and ellipses of concentration for the .675μm band versus .96μm band for data from IH-1 and M-3 sites are presented in Figure 24. As discussed in Section 5.3, the ellipses of concentration represent the areal distribution of the data obtained at each site that falls within one standard deviation of the mean. This presentation allows the evaluation of the orientation of the data clusters for the two sites relative to one another. As discussed in Section 6.1, the M-3 distribution is much more extensive than the IH-1 distribution. The IH-1 data orientation tends to be more along the axis of the .675μm band with less variation along the axis of the .96μm band. This orientation is most likely a result of the predominance of non-vegetation components for the IH-1 site. The size

of the IH-1 cluster relative to the M-3 cluster is much smaller. This is probably a function of less variation in proportions of scene components for a given scene along the transect at the IH-1 site. The larger ellipse with an orientation providing a spread of data values in both the .675μm and the .96μm bands for the M-3 site is most likely a result of wide ranges of component proportions coupled with a predominance of vegetation for each scene along the transect. Figure 25 shows the ellipses of concentration for canopy and understory categories, as discussed in Section 6.1, superimposed over the ellipse of concentration for all M-3 data. The position of the canopy and understory ellipses relative to the M-3 ellipse indicates that the canopy population contributes more to the total M-3 data set than the understory population. The separation of data populations for canopy and understory is clearly exhibited in this depiction. This separation of ellipses would be less between canopy and understory if borderline data points that did not meet the criteria discussed in Section 5.1 had not been removed. Ramifications of this potential two subpopulation condition for regression analysis on the M-3 data is discussed in the next section.

6.4 Linear Regression Model

Separate sets of linear regression equations were developed for each date that data was collected over the M-3 site and the IH-1 site. As discussed in Section 5.4, the $\alpha = .05$ level was used for the partial F criteria to determine entry and removal of variables from the regression equations. Table 5 lists the regression equations developed in the analysis of both the M-3 and the IH-1 data and the resulting R^2

values for each. The six equations developed on September 17 data exhibited generally lower R^2 values than equations developed on data from August dates. This may be a result of selective browning of the grass understory in the large meadow opening but not under the canopy, which results in a greater variance in reflectance from the understory component. The partial F value computed for entry of the proportion of understory variable into the regression equation was generally less than the partial F computed for this variable in any of the regression equations developed on August data. The phenology change in the meadow opening combined with reduced goodness of fit values for regression equations developed on the September 17 data prompted the decision not to include this data set with the August data sets for evaluation of the prediction accuracy of the regression model. There were no noticable changes in phenology of the M-3 site during the month of August, so it was decided to combine all of the August data together. As discussed in Section 5.4, one half of this combined data was randomly selected with which to develop regression equations. These regression equations were then applied to the other one half of the combined August data, to evaluate their effectiveness on a data set other than the one used to develop them. The program and procedures used in this evaluation are contained in Appendix B. The equations developed on one half of the August data and the R^2 values for each are presented in Table 5. Table 6 presents the R^2 from the regression equations, the R^2 associated with the prediction using a new data set and the standard error of prediction for each of the six equations. The procedures used to calculate the R^2 for prediction and the standard error of prediction are contained in Appendix B. The R^2 values for the regression and the prediction are

TABLE 5. Regression equations for M-3 and IH-1 sites

y_1 = .4600μm reflectance
y_2 = .5145μm reflectance
y_3 = .5500μm reflectance
y_4 = .6750μm reflectance
y_5 = .800 μm reflectance
y_6 = .9600μm reflectance

A = Zenith sun angle
C = Canopy proportion sunlit
U = Understory proportion sunlit
R = Rocks proportion

Date	Site	# of Obs.	Regression Equations	R^2
8/10/76	M-3	8	$y_1 = -.006 + .024C + .065U$	.99
			$y_2 = .0212 + .068U$	.99
			$y_3 = -.0030 + .073C + .137U$	.99
			$y_4 = .0261 + .107U$	.98
			$y_5 = .0464 + 349C + .449U$	.95
			$y_6 = .1045 + 245C + .462U$	.99
8/12/76	M-3	24	$y_1 = -.0148 + .066C + .073U$	.93
			$y_2 = -.0176 + 090C + .100U$	.94
			$y_3 = -.0190 + .129C + 144U$	.96
			$y_4 = -.0303 + .135C + .156U$	.94
			$y_5 = -.2084 + .539C + .524U + .004A$	.97
			$y_6 = -.2247 + .612C + .634U + .004A$	.97
8/21/76	M-3	31	$y_1 = -.0028 + .037C + .054U$	.96
			$y_2 = -.0037 + .061C + .078U$	.96
			$y_3 = -.0035 + .103C + .116U$	.96
			$y_4 = -.0055 + .076C + .128U$	.98
			$y_5 = -.2979 + .681C + .511U + .005A$	.94
			$y_6 = -.2357 + .613C + .546U + .004A$	.93
9/17/76	M-3	20	$y_1 = -.0363 + 040C + .076U + .001A$	.94
			$y_2 = -.0583 + .059C + .100U + .001A$	.91
			$y_3 = -.1242 + .104C + .125U + .002A$	.92
			$y_4 = -.1434 + .097C + .189U + .002A$	.91
			$y_5 = -.8558 + .558C + .430U + .014A$	.86
			$y_6 = -.8727 + .560C + .524U + .014A$	.90

TABLE 5. Regression equations for M-3 and IH-1 sites (Continued)

Date	Site	# of Obs.	Regression Equations	R^2
½ August Data	M-3	32	$y_1 = -.0078 + .052C + .065U$	.93
			$y_2 = -.0092 + .076C + .091U$	.94
			$y_3 = -.0094 + .115C + .133U$	.94
			$y_4 = -.0161 + .109C + .142U$	.94
			$y_5 = -.2048 + .577C + .524U$	.92
			$y_6 = .0148 + .509C + .551U$	.95
9/13/76	IH-1	24	$y_1 = .0208 + .351R + .071U - .001A$	.87
			$y_2 = .0281 + .388R + .078U - .001A$	.86
			$y_3 = .0382 + .079C + .418R + .090U - .001A$	.85
			$y_4 = .0503 + .588R + .110U - .001A$	.88
			$y_5 = .0528 + .435C + .204U$	.46
			$y_6 = .0410 + .426C + .270U$	.55

TABLE 6. Comparison of regression and prediction R2 values (August M-3 data)

λ	R^2 Regression	R^2 Prediction	Standard Error of Predictions
.4600μm	.93	.92	.00557
.5145μm	.94	.92	.00725
.5500μm	.94	.94	.00904
.6750μm	.94	.95	.00969
.8000μm	.92	.86	.04477
.9600μm	.95	.93	.03933

within 2 percent except for the equation predicting reflectance for the .8000μm band when the R^2 for prediction is 6 percent below the R^2 for regression. The plots of coefficients for the canopy and understory components for various dates of data acquisition (Figure 26 and 27) do not include the August 10 data set. The reason for this is that one of the 6 equations developed on this data did not include canopy proportion as a significant independent variable. This is caused by the lack of forested data points present in this data set. Generally, plots of the coefficients for both canopy and understory (Figure 26 and 27) follow a pattern representative of a reflectance curve for each of those components. The plot of the canopy coefficients exhibits more variation than the understory coefficients. This probably is a function of the variability of the shadow component within the canopy which induces potentially larger error for the proportion estimates for canopy than is present for understory.

R^2 values from regression equations developed on the IH-1 data set are roughly 10 percent below R^2 values for comparable equations developed on M-3 data for the visible wavelength (.46, .5145, .55, .675μm). The R^2 values for the IH-1 equations predicting reflectance in the .80μm and .96μm bands are very low. The R^2's are .46 and .55 respectively.

The high R^2 values for the majority of the equations developed on M-3 site data are somewhat misleading. This equation was developed on what might be termed a choice data set. The transect with its heavily wooded section and open meadow areas provides a two sub-population condition as discussed previously. This results in a wide range of proportion of components and subsequent wide ranges in spectral

reflectance which lend themselves to regression analysis. In addition, the scenes along the M-3 site are relatively uncomplicated spectrally with three primary scene components. Two of the components, canopy and understory, are spectrally similar and the third component, shadows, exhibits relatively homogenous reflectance characteristics whether associated with the canopy or the understory. Conversely, the IH-1 site exhibits a more complex scene. There is less variation in scene component proportions in conjunction with a wide variation in spectral characteristics of those components. The complexity of the ground surface below the canopy with numerous white rock fragments and combinations of bare soil/litter, and small clumps of juniper and sage makes it very difficult to estimate the proportions of the components present. These components, unlike those of the M-3 site, are spectrally quite different from one another which tends to magnify any proportion estimation errors in the subsequent regression analysis. As discussed in Chapter 4, the error between operators in estimating proportions of scene components for the IH-1 site was more than twice that of the M-3 site estimates. Error introduced from estimation of spectral irradiance is quite small and should have minimal effect on the regression analysis results in the visible wavelengths and only a minor effect for the near infrared bands. The sun angle independent variable was always the final variable entered for those equations in which it met the $\alpha = .05$ F criteria. It appears that it was only significant in equations which exhibited a lower R^2 value after the component proportion variables were already in the equation.

7.0 CONCLUSIONS AND RECOMMENDATIONS

Results of the attempts to relate scene component proportions to scene spectral response were mixed, with very good predictability for the M-3 site and lesser reliability for the IH-1 site. More research needs to be done to verify the suspected reasons for the variations between results obtained over the two sites. Initial results obtained in this study give sufficient credibility to the linear relationship theory between scene component proportions and scene spectral response to warrant continued study in this area. However, based on the results from this study, it appears that the three dimensional effects of the scene structure must somehow be incorporated into the linear regression model. Most studies relating scene component proportions to reflectance prior to this experiment have disregarded the three dimensional structural effects of the scene. In this study, the three dimensional structure of the scene was considered indirectly by the shadowing which resulted. Actually, shadowing is the result of three dimensional structure of the scene, sun angle and azimuth, slope and aspect. Shadowing has a pronounced effect on scene spectral response especially in forested areas. Three dimensional structure of a forested scene may affect spectral response in ways other than just shadowing. These include the effect of leaf-angle distribution relative to incoming irradiance, and spatial arrangement within and between trees in scene resulting in variation in the reflectance characteristics. However, it appears that shadowing by far exerts the greatest effect on scene spectral response relative to other structural manifestations in a forest situation. Shadowing and other three dimensional effects are present in all natural scenes, but are less pronounced where the vertical component of

scene structure is small. Treating shadows as a scene component may not be the best method of approaching the three dimensional structure problem, but it has provided a measurable parameter to account for a portion of structural effect for the purposes of this study. Shadows may need to be subdivided as scene components, particularly where the shadowed area is not relatively homogenous spectrally such as for the IH-1 site.

The key to effectiveness of the approach used in this study seems to be the ability to effectively isolate those components which account for the majority of the scene spectral response and then estimate their proportion with reasonable accuracy. If this can be done, then results from this study indicate that reasonable mathematical relationships can be established to relate scene component proportions to the scene spectral response.

Additional studies combined with alterations in certain approaches implemented in this study should help to further define the relationships between scene components and spectral reflectance. Two additional studies that would be desirable to define the effects of the three dimensional structure of a scene are: 1) a well defined sun angle experiment in which reflectance is measured from a given scene over as wide a range of sun angles as possible, and 2) further study of the physical structure (geometry) of various canopy types to better understand the interaction of light with the canopy. Techniques developed by Berry (1976) for determining canopy geometry in wheat might be extended to forest canopies.

Several modifications to approaches used in this study may help to better define the initial results obtained in this study. The density slicing approach provides a rapid means of estimating proportions of

components defined by their spectral contributions to the total scene reflectance. Accuracy in the estimates of proportions might be improved with the use of color or color IR film for density slicing. It is possible to density slice individual layers of color or color IR film (McDowell and Specht, 1974) thereby effectively providing an image of the scene in three wavelength bands corresponding to the sensitivity of the film layers. This may result in better density separation for scene components that tend to have overlapping densities on a broad band image. Better separation could significantly improve proportion estimates especially for more complex scenes.

This study has indicated a need to incorporate shadows as a surrogate for three dimensional structure into the linear regression relationships. Using similar measurement procedures applied to aircraft systems, it would be highly advantageous to evaluate this requirement as a function of altitude, i.e. spatial resolution. It may be possible, for example, that a general canopy component may be defined which does not require separation into shadowed versus unshadowed components.

REFERENCES CITED

Behre, C. H. 1953. Geology and Ore Deposits of the West Slope of the Mosquito Range: U. S. Geological Survey Ref. Paper 235, 176 pp.

Berry, J. K. 1976. Extracting Scene Feature Vectors Through Modeling. Ph.D. Dissertation. Department of Earth Resources, Colorado State University, Fort Collins, Colorado 111 pp.

Burroughs, E. R. 1971. Short-Wave Reflectivity of Lodgepole Pine. Ph. D. Dissertation. Colorado State University, Fort Collins, Co.

Coggeshall, M. E. and R. M. Hoffer. 1973. Basic Forest Cover Mapping Using Digitized Remote Sensor Data and ADP Techniques. The Laboratory for Applications of Remote Sensing, Purdue University, West Lafayette, Indiana. 131 pp.

Davis, J. C. 1973. Statistics and Data Analysis in Geology. John Wiley and Sons, Inc. New York, New York. 550 pp.

Draper, N. R. and H. Smith. 1966. Applied Regression Analysis. John Wiley and Sons, Inc. New York, New York. 407 pp.

Driscoll, R. S., and R. E. Francis. 1970. Multistage, Multiseasonal and Multiband Imagery to Identify and Qualify Non-Forest Vegetation Resources. Remote Sensing Applications in Forestry. Annual Progress Report. 71 pp.

Horwitz, H. M., R. F. Nalepka, P. D. Hyde and J. P. Morgenstern. 1971. Estimating the Proportions of Objects Within a Single Resolution Element of a Multispectral Scanner. Proceedings of the Seventh International Symposium on Remote Sensing of the Environment. Ann Arbor, Michigan p. 1307-1320.

International Mathematical and Statistical Libraries (IMSL), Inc. 1975. Vol. II. Houston, Texas.

Leonard, R. E. and A. R. Eschner. 1968. A Treetop Tramway System for Meterological Studies U. S. Forest Service Research Paper NE-92 Northeastern Experiment Station. 10 pp.

Leschack, L. A. 1971. Automatic Data Processing of Forest Imagery. Photogramm Eng. 37:885-896.

McDowell, D. Q. and M. R. Specht. 1974. Determination of Spectral Reflectance Using Aerial Photographs. Photogramm. Eng. 40:559-568.

Mead, R. A. 1974. Factors Affecting Computer Recognition of Ponderosa Pine from ERTS-1 Imagery. Master's Thesis. Department of Earth Resources, Colorado State University, Fort Collins, Colorado 85pp.

Oliver, R. E. and J. A. Smith. 1974. A Stochastic Canopy Model of Diurnal Reflectance. Final Report, DAHC04 74 G)))1, U. S. Army Research Office, Durham, N. C., 82 pp.

Pace, W. H. and D. M. Detchmendy. 1972. A Model for Spectral Signature Variability for Mixtures. Remote Sensing of Earth Resources, Vol. I. F. Shahrokhi, editor. Tullahoma, Tennessee. p. 596-620.

_____. 1973. A Fast Algorithm for the Decomposing of Multispectral Data Into Mixtures. Remote Sensing of Earth Resources, Vol. II. F. Shahrokhi, editor. Tullahoma, Tennessee. p. 831-848.

Pearson, R. 1973. Remote Multispectral Sensing of Biomass. Ph.D. Dissertation. Colorado State University, Fort Collins, Colorado. 99 pp.

Ranson, K. J. 1975. Computer Assisted Classification of Mixtures With Simulated Spectral Signatures. Master's Thesis. Department of Earth Resources, Colorado State University, Fort Collins, Colorado, 92 pp.

Reeves, R. G., A. Anson and D. Landen. 1975. Manual of Remote Sensing. Vol. I. American Society of Photogrammetry. Falls Church, Virginia. 867 pp.

Silvestro, F. B. 1969. Multispectral Photographic Determination of Reflectance. Photogramm. Eng., 35(3):258-262.

Smith, J. A. and R. E. Oliver. 1974. Effects of Changing Canopy Directional Reflectance on Feature Selection. Applied Optics. Vol. 13. p. 1599-1604.

Spatial Data Systems Technical Manual. Model 401/703 Data Color/Edge Enhancer System.

Tektronix Inc. 1972. Technical Manual. Model J-16 Digital Photometer.

APPENDIX A

DATA LISTINGS

1. Physical Stand Characteristics; M-3 and IH-1
2. Reflectance and Component Proportion Data

8/10/76 - M-3

8/12/76 - M-3

8/21/76 - M-3

9/17/76 - M-3

9/13/76 - IH-1

1. Physical Stand Characteristics

DATA TYPE: Tree Inventory
SITE : M-3
DATE : 8/3/76

Tree Tag No.	Height(Ft.)	DBH(In.)	Age(Yrs.)
1	12	3.0	
2	18	4.7	
3	15	3.5	
4	10	1.9	
5	20	5.6	
6	14	3.1	
7	8	1.0	
8	14	3.3	
9	26	8.0	
10	10	1.0	
11	24	5.3	
12	27	8.1	
13	23	4.1	
14	24	6.6	
15	15	3.2	
16	31	12.3	50
17	21	7.2	
18	14	3.7	
19	17	4.2	
20	11	3.8	
21	25	5.8	
22	19	4.4	
23	15	3.9	
24	15	5.2	
25	9	1.8	
26	10	3.3	
27	24	7.5	42
28	18	7.3	
29	28	7.0	
30	24	6.8	
31	14	3.6	31
32	23	3.1	
33	19	5.7	
34	17	5.6	
35	21	7.1	
36	22	7.2	
37	21	5.2	
38	16	4.5	
39	20	5.0	
40	15	3.1	
41	8	1.4	
42	24	6.7	
43	15	5.5	
44	11	1.9	

1. Physical Stand Characteristics (Continued)

DATA TYPE: Tree Inventory
SITE : M-3
DATE : 8/3/76

Tree Tag No.	Height(Ft.)	DBH(In.)	Age(Yrs.)
45	9	2.2	
46	20	7.1	
47	16	6.0	
48	9	.9	
49	12	3.4	
50	21	4.1	
51	24	5.3	
52	15	3.3	
53	19	6.7	
54	13	4.8	
55	9	1.5	
56	19	6.7	
57	8	1.0	
58	12	3.6	
59	11	2.5	
60	23	6.2	
61	25	6.8	
62	23	5.4	34
63	8	.9	
64	16	4.4	
65	10	1.2	17
66	10	1.8	
67	21	7.4	
68	26	7.3	
69	27	6.4	
70	18	4.2	
71	14	3.4	
72	13	2.8	
73	13	2.5	
74	18	6.3	
75	23	6.6	
76	15	2.6	
77	17	4.9	
78	18	5.1	
79	9	2.6	
80	22	5.8	30
81	23	6.4	
82	27	7.0	
83	28	8.6	
84	8	1.1	
85	12	3.6	
86	26	6.8	
87	26	5.1	
88	8.5	2.2	

1. Physical Stand Characteristics (Continued)

DATA TYPE: Tree Inventory
SITE : M-3
DATE : 8/3/76

Tree Tag No.	Height(Ft.)	DBH(In.)	Age(Yrs.)
89	13	2.6	
90	23	9.7	
91	27	7.0	
92	17	4.5	
93	9	1.5	

1. Physical Stand Characteristics

DATA TYPE: Tree Inventory
SITE : IH-1
DATE : 8/19/76

A and B Indicate Dicotomous Trunks

Tree Tag No.	Height(Ft.)	DBH(In.)	Age(Yrs.)
1	17	3.2	
2	14	2.7	
3	9	2.2	
4	17	4.1	
5	15	4.6	
6	8	1.3	
7	8	1.2	
8	12	2.6	
9	19	4.0	
10	13	2.1	24
11	22	3.2	
12	26	4.3	
13	29	8.2	
14A	43	7.6	
14B	43	9.2	69
15	13	2.1	
16	15	2.8	
17	13	2.3	
18	30	5.3	
19A	36	8.8	
19B	36	9.0	
20	18	2.9	41
21	17	2.8	
22	21	4.1	
23	11	1.8	
24	17	2.9	
25	17	2.5	
26	15	2.3	
27	15	2.4	
28	17	2.9	
29	20	3.1	
30A	18	3.0	37
30B	18	4.1	
31	21	2.6	
32	14	4.0	
33	22	4.2	
34	17	5.3	
35	24	5.7	
36	28	5.7	
37	9	1.6	
38	17	3.9	
39	10	2.2	

1. Physical Stand Characteristics (Continued)

DATA TYPE: Tree Inventory
SITE : IH-1
DATE : 8/19/76

A and B Indicate Dicotomous Trunks

Tree Tag No.	Height(Ft.)	DBH(In.)	Age(Yrs.)
40	10	2.2	24
41A	19	4.0	
41B	19	2.2	
42	17	3.3	
43	22	4.2	
44	21	3.6	
45	22	3.6	
46	20	2.8	
47	23	5.0	
48	20	3.6	
49	14	3.5	
50	12	2.0	26
51	19	4.4	
52	14	2.2	
53	19	4.7	
54	15	3.1	
55	15	2.9	
56	25	6.5	
57	16	3.4	
58	18	3.4	
59	12	2.9	
60	22	4.2	38
61	18	2.1	
62	10	2.2	
63	17	3.3	
64	19	3.3	
65	19	3.4	
66	9	1.5	
67	14	3.4	
68	23	5.3	
69	11	1.7	
70	22	4.0	35
71	26	6.6	
72	8	1.6	
73	13	2.7	
74	15	3.4	
75	30	6.3	
76	25	4.2	
77	30	4.9	
78	26	5.3	
79	18	3.1	
80	26	4.6	41

1. Physical Stand Characteristics (Continued)

DATA TYPE: Tree Inventory
SITE : IH-1
DATE : 8/19/76

A and B Indicate Dicotomous Trunks

Tree Tag No.	Height(Ft.)	DBH(In.)	Age(Yrs.)
81	20	3.3	
82	24	4.4	
83	21	5.3	
84	14	2.2	
85	18	3.6	
86	14	1.9	
87A	38	6.2	38
87B	38	5.7	
87C	38	3.0	
87D	38	4.6	
87E	38	12.0	
88	14	2.5	
89	14	4.9	
90	22	4.2	42
91A	20	3.6	
91B	20	3.4	
88A	17	3.0	
88B	17	2.6	
92	21	4.4	
93	11	1.9	
94	35	5.4	

2. Reflectance and Component Proportion Data

SITE: M-3 DATE: 08/10/76

Local Time	Transect Position	Zenith Sun Angle	Scene Component Proportions				Spectral Reflectance					
			Shadow	Understory	Rocks	Canopy	λ1 μm .4600	λ2 μm .5145	λ3 μm .5500	λ4 μm .6750	λ5 μm .8000	λ6 μm .9600
1029	090 ft.	40.3	.44	.17	--	.39	.019	.028	.045	.036	.238	.258
1030	080 ft.	40.1	.28	.05	--	.67	.018	.029	.051	.036	.292	.283
1032	070 ft.	39.7	.42	.09	--	.49	.016	.025	.044	.032	.283	.284
1033	060 ft.	39.6	.10	.82	--	.08	.053	.072	.108	.104	.399	.491
1034	050 ft.	39.4	.02	.97	--	.01	.063	.087	.130	.127	.508	.549
1036	040 ft.	39.0	.02	.98	--	.00	.065	.089	.131	.134	.491	.557
1039	030 ft.	38.5	.10	.78	--	.12	.052	.079	.118	.118	.450	.517
1055	020 ft.	35.8	.40	.17	--	.43	.022	.035	.056	.050	.283	.296

SITE: M-3 DATE: 08/12/76

Local Time	Transect Position	Zenith Sun Angle	Scene Component Proportions				Spectral Reflectance					
			Shadow	Understory	Rocks	Canopy	λ1 μm .4600	λ2 μm .5145	λ3 μm .5500	λ4 μm .6750	λ5 μm .8000	λ6 μm .9600
0917	120 ft.	54.0	.79	.06	--	.15	.005	.009	.017	.012	.132	.139
0919	110 ft.	53.7	.76	.04	--	.20	.006	.011	.022	.013	.169	.167
0923	100 ft.	52.9	.74	.03	--	.23	.006	.010	.021	.013	.164	.162
0925	90 ft.	52.5	.68	.05	--	.27	.009	.016	.030	.021	.198	.206
0927	80 ft.	52.1	.48	.03	--	.49	.014	.025	.043	.031	.030	.302
0929	70 ft.	51.8	.64	.01	--	.35	.009	.016	.032	.019	.254	.245
0930	60 ft.	51.6	.66	.33	--	.01	.009	.015	.026	.022	.150	.169
0932	50 ft.	51.2	.06	.09	--	.01	.040	.064	.105	.102	.506	.571
0934	40 ft.	50.8	.01	.98	--	.01	.056	.078	.121	.123	.494	.575
0956	20 ft.	46.7	.38	.11	--	.51	.024	.036	.063	.049	.337	.349
0959	30 ft.	46.2	.04	.94	--	.02	.059	.087	.133	.131	.534	.628
1000	040 ft.	46.0	.01	.99	--	.00	.061	.087	.129	.131	.535	.634
1001	050 ft.	45.8	.03	.96	--	.01	.054	.075	.116	.113	.489	.588
1003	060 ft.	45.4	.32	.65	--	.03	.029	.042	.068	.064	.319	.370
1005	070 ft.	45.1	.54	.07	--	.39	.011	.018	.033	.022	.242	.236
1006	080 ft.	44.9	.35	.06	--	.59	.017	.027	.047	.033	.290	.296
1008	090 ft.	44.5	.52	.06	--	.42	.015	.023	.036	.027	.208	.223
1010	100 ft.	44.2	.56	.04	--	.40	.011	.017	.032	.022	.200	.214
1011	110 ft.	44.0	.67	.01	--	.32	.009	.015	.027	.018	.186	.189
1103	060 ft.	35.1	.08	.91	--	.01	.057	.077	.114	.114	.416	.509
1105	050 ft.	34.8	.01	.98	--	.01	.060	.084	.126	.126	.486	.549
1107	040 ft.	34.5	.01	.99	--	.00	.062	.089	.129	.134	.452	.524
1108	030 ft.	34.3	.14	.05	--	.81	.057	.078	.115	.119	.410	.488
1109	020 ft.	34.1	.42	.23	--	.35	.022	.033	.051	.049	.247	.269

SITE: M-3 DATE: 08/21/76

Local Time	Transect Position	Zenith Sun Angle	Scene Component Proportions				Spectral Reflectance					
			Shadow	Understory	Rocks	Canopy	λ1 μm .4600	λ2 μm .5145	λ3 μm .5500	λ4 μm .6750	λ5 μm .8000	λ6 μm .9600
0837	140 ft.	63.8	.56	.02	--	.42	.016	.030	.057	.036	.402	.337
0840	130 ft.	63.2	.58	.07	--	.35	.012	.020	.037	.026	.294	.248
0842	120 ft.	62.8	.85	.01	--	.14	.004	.008	.014	.011	.110	.102
0844	110 ft.	62.4	.81	.01	--	.18	.004	.009	.018	.011	.141	.121
0846	100 ft.	62.0	.91	.01	--	.08	.002	.005	.010	.006	.089	.079
0848	90 ft.	61.7	.82	.01	--	.17	.004	.010	.020	.012	.142	.120
0851	80 ft.	61.1	.61	.04	--	.35	.009	.018	.034	.023	.231	.209
0852	70 ft.	60.9	.61	.09	--	.30	.011	.019	.039	.025	.301	.256
0855	60 ft.	60.3	.95	.05	--	.00	.003	.004	.007	.004	.054	.050
0858	50 ft.	59.7	.31	.69	--	.00	.026	.039	.063	.071	.346	.344
0900	40 ft.	59.4	.02	.98	--	.00	.044	.070	.104	.118	.501	.509
0902	30 ft.	59.0	.02	.96	--	.02	.050	.073	.112	.123	.529	.541
0904	20 ft.	58.6	.34	.51	--	.15	.027	.040	.068	.061	.399	.372
0924	135 ft.	54.8	.45	.02	--	.53	.021	.035	.060	.042	.384	.335
0928	125 ft.	54.1	.75	.02	--	.23	.008	.013	.024	.016	.206	.175
0932	115 ft.	53.3	.72	.02	--	.26	.007	.013	.025	.016	.171	.154
0935	105 ft.	52.7	.75	.01	--	.24	.007	.013	.026	.016	.182	.159
0938	95 ft.	52.2	.70	.01	--	.29	.008	.013	.024	.017	.163	.150
0940	85 ft.	51.8	.58	.06	--	.36	.014	.024	.041	.030	.248	.223
0943	75 ft.	51.3	.43	.01	--	.56	.017	.030	.055	.037	.364	.322
0945	65 ft.	50.9	.82	.15	--	.03	.005	.008	.015	.013	.102	.097
0948	55 ft.	50.3	.17	.83	--	.00	.038	.052	.087	.090	.425	.428
0950	45 ft.	50.0	.03	.96	--	.01	.053	.075	.110	.121	.450	.488
0953	35 ft.	49.4	.01	.99	--	.00	.058	.082	.121	.134	.457	.498
0955	25 ft.	49.1	.22	.60	--	.18	.043	.061	.094	.096	.412	.428
0958	15 ft.	48.5	.61	.02	--	.37	.013	.019	.031	.025	.169	.163
1020	140 ft.	44.6	.35	.15	--	.50	.026	.046	.077	.059	.386	.378
1022	130 ft.	44.3	.62	.01	--	.37	.012	.019	.034	.023	.260	.233

SITE: M-3 DATE: 08/21/76

Local Time	Transect Position	Zenith Sun Angle	Scene Component Proportions				Spectral Reflectance					
			Shadow	Understory	Rocks	Canopy	λ1 μm .4600	λ2 μm .5145	λ3 μm .5500	λ4 μm .6750	λ5 μm .8000	λ6 μm .9600
1024	120 ft.	43.9	.54	.02	--	.44	.010	.016	.028	.022	.172	.166
1026	110 ft.	43.6	.61	.01	--	.38	.009	.015	.028	.019	.180	.167
1029	100 ft.	43.0	.58	.03	--	.39	.012	.018	.031	.024	.194	.187

SITE: M-3 DATE: 09/17/76

Local Time	Transect Position	Zenith Sun Angle	Scene Component Proportions				Spectral Reflectance					
			Shadow	Understory	Rocks	Canopy	λ1 μm .4600	λ2 μm .5145	λ3 μm .5500	λ4 μm .6750	λ5 μm .8000	λ6 μm .9600
0912	140 ft.	65.1	.36	.09	--	.55	.027	.042	.073	.055	.459	.456
0915	130 ft.	64.6	.70	.10	--	.20	.011	.016	.030	.019	.236	.223
0918	120 ft.	64.0	.65	.11	--	.24	.010	.015	.027	.019	.173	.171
0920	110 ft.	63.7	.75	.17	--	.08	.010	.016	.030	.019	.202	.197
0923	100 ft.	63.1	.81	.02	--	.17	.008	.011	.019	.013	.132	.131
0924	90 ft.	62.9	.51	.07	--	.42	.016	.027	.049	.034	.283	.284
0926	80 ft.	62.6	.36	.09	--	.55	.021	.033	.061	.042	.376	.369
0927	70 ft.	62.4	.84	.14	--	.02	.007	.009	.012	.012	.074	.083
0928	60 ft.	62.2	.35	.64	--	.01	.041	.053	.068	.102	.289	.352
0932	50 ft.	61.5	.03	.96	--	.01	.077	.099	.127	.204	.457	.552
0957	120 ft.	57.1	.48	.12	--	.40	.011	.016	.026	.023	.147	.151
1003	110 ft.	56.1	.55	.02	--	.43	.015	.017	.032	.025	.191	.187
1007	100 ft.	55.4	.66	.08	--	.26	.011	.016	.026	.024	.147	.154
1008	90 ft.	55.2	.42	.08	--	.50	.018	.026	.043	.035	.225	.228
1010	80 ft.	54.9	.53	.04	--	.43	.018	.026	.045	.034	.261	.249
1014	70 ft.	54.2	.52	.33	--	.15	.017	.022	.033	.035	.153	.164
1018	60 ft.	53.6	.04	.96	--	.00	.054	.068	.087	.115	.293	.351
1022	50 ft.	52.9	.22	.78	--	.00	.050	.059	.071	.098	.215	.282
1024	40 ft.	52.6	.28	.66	--	.06	.049	.076	.075	.104	.243	.293
1025	30 ft.	52.4	.44	.05	--	.51	.012	.017	.028	.024	.153	.154

SITE: IH-1 DATE: 09/13/76

Local Time	Transect Position	Zenith Sun Angle	Scene Component Proportions				Spectral Reflectance					
			Shadow	Understory	Rocks	Canopy	λ1 μm .4600	λ2 μm .5145	λ3 μm .5500	λ4 μm .6750	λ5 μm .8000	λ6 μm .9600
0948	130 ft.	57.3	.27	.54	.09	.10	.057	.066	.080	.099	.223	.249
0949	120 ft.	57.2	.36	.45	.08	.11	.039	.043	.054	.071	.137	.163
0951	110 ft.	56.8	.31	.41	.07	.21	.041	.049	.067	.071	.224	.238
1006	100 ft.	54.2	.28	.39	.08	.25	.041	.053	.079	.077	.294	.297
1017	90 ft.	52.3	.55	.24	.06	.15	.034	.036	.047	.058	.133	.142
1019	80 ft.	52.0	.37	.37	.02	.24	.024	.034	.061	.049	.260	.255
1023	70 ft.	51.3	.27	.46	.10	.17	.065	.080	.102	.123	.277	.298
1027	60 ft.	50.7	.18	.68	.11	.03	.084	.094	.103	.133	.208	.243
1033	50 ft.	49.7	.42	.46	.06	.06	.045	.051	.059	.079	.149	.168
1035	40 ft.	49.4	.43	.37	.05	.15	.030	.034	.051	.055	.156	.164
1037	30 ft.	49.1	.36	.32	.04	.28	.027	.033	.050	.052	.189	.196
1039	20 ft.	48.8	.31	.38	.05	.26	.035	.041	.056	.066	.183	.196
1131	135 ft.	41.5	.49	.35	.05	.11	.031	.040	.061	.071	.154	.174
1153	125 ft.	39.3	.38	.57	.04	.01	.053	.061	.069	.092	.152	.183
1209	105 ft.	37.6	.31	.31	.08	.30	.047	.060	.089	.086	.300	.311
1212	95 ft.	37.4	.25	.49	.07	.19	.069	.079	.096	.123	.220	.251
1220	85 ft.	36.8	.36	.46	.05	.13	.047	.054	.077	.084	.233	.242
1305	75 ft.	35.1	.56	.27	.04	.13	.034	.042	.060	.065	.202	.203
1311	65 ft.	35.1	.51	.29	.07	.13	.048	.054	.066	.085	.139	.145
1314	55 ft.	35.1	.22	.65	.09	.04	.088	.098	.114	.150	.217	.248
1320	45 ft.	35.2	.18	.64	.09	.09	.060	.073	.095	.113	.245	.258
1325	35 ft.	35.3	.45	.40	.08	.07	.048	.055	.069	.088	.186	.194
1357	25 ft.	36.8	.72	.16	.02	.10	.022	.029	.042	.043	.169	.163

APPENDIX B

PROGRAM LISTINGS

1. Program "Ellipse"
2. Program "Prediction Evaluation"
3. Program "Sun Angle"

Program "Ellipse"

Program "Ellipse" is a program which plots ellipses of concentration for two variables. The program uses means of each data set, eigenvalues and eigenvectors to compute the dimensions and orientation of the ellipse. The ellipse is then graphically displayed on an x, y coordinate system of dimensions selected by the user.

```
1   REM PROGRAM ELLIPSE
3   PRINT "THIS PROGRAM COMPUTES AND PLOTS AN ELLIPSE DESCRIBING"
4   PRINT "A DATA POPULATION."
5   PRINT "INPUT DATA ON THE KEYBOARD AS REQUESTED DURING EXECUTION."
9   PRINT " "
10  PRINT  "ENTER PLOTTING SCALE LIMITS:XMIN,XMAX,YMIN,YMAX"
15  PRINT  " "
20  INPUT  X1,X2,Y1,Y2
30  SCALE  X1,X2,Y1,Y2
40  PRINT  "ENTER X AND Y AXIS TIC INTERVALS:T1,T2"
45  PRINT  " "
50  INPUT  T1,T2
60  XAXIS  Y1,T1,X1,X2
70  XAXIS  Y2,T1,X1,X2
80  YAXIS  X1,T2,Y1,Y2
90  YAXIS  X2,T2,Y1,Y2
95  DEG
100 PRINT  "ENTER MEANX,MEANY,LARGEST E-VALUE, SMALLEST E-VALUE"
115 PRINT  " "
116 PRINT  " "
117 INPUT  01,02,A,B
118 PRINT  "ENTER EIGENVECTOR ELEMENTS ASSOCIATED WITH LARGEST EIGENVALUE"
119 PRINT  " "
120 INPUT  Q1,Q2
124 PLOT  01,02,1
125 PLOT  01,02,2
126 A=SQR(A)
127 B=SQR(B)
129 D=A
130 C=-A
131 IF Q1=0 THEN 137
132 S=ATN(Q2/Q1)
135 GOTO 140
137 S=90
140 PEN
145 PEN
150 FOR X=C TO D STEP A/5
160 Y=B*SQR(1-X↑2/A↑2)
165 X1=X*COS(S)-Y*SIN(S)
167 Y1=X*SIN(S)+Y*COS(S)
169 IF X=C THEN 175
170 PLOT X1+01,Y1+02,+2
173 GOTO 230
175 PLOT X1+01,Y1+02,1
230 NEXT X
235 PEN
240 FOR X=C TO D STEP A/5
245 Y=-B*SQR(1-X↑2/A↑2)
250 X1=X*COS(S)-Y*SIN(S)
255 Y1=X*SIN(S)+Y*COS(S)
256 IF X=C THEN 262
260 PLOT X1+01,Y1+02,+2
261 GOTO 280
262 PLOT X1+01,Y1+02,1
```

```
280 NEXT X
290 PEN
291 PRINT "IF ADDITIONAL PLOTS ARE DESIRED INPUT 1"
292 PRINT "IF YOU WISH TO USE THE KEYBOARD AS A TYPEWRITER TO LABEL THE"
293 PRINT "PLOTS INPUT 2"
294 PRINT " "
295 INPUT W
296 IF W=1 THEN 100
297 PRINT "NOTE YOU WILL HAVE TO ADJUST THE GRAPH LIMITS TO BE ABLE TO"
298 PRINT "LABEL YOUR X AND Y AXES."
299 PRINT " "
300 LETTER
305 END
```

Program Prediction Evaluation

This program provides a means of applying a regression equation developed on one set of data to a second data set to evaluate the prediction accuracy of the equation. The program computes a standard error of prediction, a standard error of reduction, the standard deviation for the second data set, the correlation coefficient of prediction and the R^2 of the prediction. The following discussion presents the methods used to calculate the statistics listed.

The standard error of prediction (S pred.) is calculated as folows:

$$S\ pred = \sqrt{\sum_{i=1}^{n} \frac{(y_i,\ meas. - y_i,\ pred.)^2}{n}}$$

y_i meas. = measured reflectance for band i second data set

y_i pred. = predicted reflectance for band i using regression equation applied to second data set

n = size of second data set

The standard error of reduction (S_r) for the second data set is calculated by the equation:

$$S_r = \sqrt{\sum_{i=1}^{n} \frac{(y_i,\ meas. - y_i,\ pred.)^2}{n-1}}$$

The standard deviation (S_y) of the reflectance y_i of the second data set is calculated by the equation:

$$S_y = \sqrt{\sum_{i=1}^{n} \frac{(y_i,\ meas. - y_i,\ mean)^2}{n-1}}$$

y_i = mean of reflectance values for band i, second data set

The correlation coefficient of prediction (R) is calculated using the equation:

$$R = \sqrt{1 - \frac{S_r^2}{S_y^2}}$$

and the prediction R^2 is the square of the correlation coefficient of prediction.

```
05  "PROGRAM PREDICTION EVALUATION"
10  DIM Y(50)
20  DISP "WAVELENGTH OF REFLECTANCE MEAS.";
30  INPUT W
40  DISP "COEFFICIENT FOR PROP. UNDERSTORY";
50  INPUT C2
60  DISP "COEFFICIENT FOR PROP. CANOPY";
70  INPUT C3
80  DISP "INTERCEPT CONSTANT";
90  INPUT C1
100 DISP  "NUMBER OF OBSERVATIONS";
110 INPUT  N
120 PRINT "WAVELENGTH=";W;"MICROMETERS"
130 PRINT "INTERCEPT=";C1
140 PRINT "UNDERSTORY COEFFICIENT=";C2
150 PRINT "CANOPY COEFFICIENT=";C3
160 PRINT "NUMBER OF OBSERVATIONS=";N
170 S=0
180 S1=0
190 PRINT
200 PRINT
210 WRITE (15,520)
220 WRITE (15,530)
230 FOR I=1 TO N
240 DISP "REFLECTANCE=";
250 INPUT Y(I)
260 DISP "PROPORTION UNDERSTORY=";
270 INPUT U
280 DISP "PROPORTION CANOPY=";
290 INPUT C
300 Y1=C1+C2*U+C3*C
310 S=S+(Y(I)-Y1)↑2
320 S1=S1+Y(I)
330 D=Y(I)-Y1
340 WRITE (15,540)I;U;C;Y(I);Y1;D
350 NEXT I
360 M=S1/N
370 S1=0
380 FOR J=1 TO N
390 S1=S1+(Y(J)-M)↑2
400 NEXT J
410 E=SQR(S/(N-1))
420 E1=SQR(S1/(N-1))
430 E2=SQR(S/N)
440 R=SQR(1-(E↑2)/(E1↑2))
450 R2=R↑2
460 PRINT
470 PRINT
480 PRINT "STANDARD DEVIATION OF MEASURED REFLECTANCE=";E1
490 PRINT "STANDARD ERROR OF PREDICTION=";E2
500 PRINT "CORRELATION COEFFICIENT=";R
510 PRINT "GOODNESS OF FIT (R SQUARED) =";R2
520 FORMAT "OBS.",5X,"PROPORTION",5X,"PROPORTION",7X,"MEAS",11X,"CALC",
    8X,"ERROR
```

```
530 FORMAT "NUM.",5X,"UNDERSTORY",7X,"CANOPY",6X,"REFLECTANCE",4X,"
    "REFLECTANCE"
540 FORMAT F3.0,8X,F5.2,10X,F5.2,8X,F8.5,7X,F8.5,4X,F8.5
550 END
```

Program Sun Angle

This program computes the Zenith Sun Angle for a flat surface. The inputs to the program include: 1) Latitude, 2) Date, 3) Declination, 4) Equation of Time, 5) Local Time, and 6) Whether time is standard or daylight savings. The program will compute a Zenith Sun Angle for each local time of day that is input. Zenith sun angle is the angle of the sun measured from the normal to a horizontal surface.

```
10  PRINT "PROGRAM SUN ANGLE"
20  PRINT
30  PRINT "    THIS PROGRAM CALCULATES THE ZENITH ANGLE OF THE SUN FOR A"
40  PRINT "    GIVEN THE TIME OF DAY"
50  PRINT
60  PRINT "     INPUTS INCLUDE THE FOLLOWING:  LATITUDE IN DECIMAL FORM;
              DATE"
70  PRINT "    6 DIGITS; DECLINATION OF THE SUN FOR THE DESIRED DATES;
              LOCAL"
80  PRINT "     TIME;  STANDARD/DAYLIGHT SAVINGS TIME ?; EQUATION OF TIME"
90  PRINT "     IN DECIMAL FORM"
100 PRINT
110 PRINT
120 PRINT "TO CHANGE DATE, DECLINATION, AND EQUATION OF TIME PRESS (CONT)
        130"
130 PRINT
140 PRINT
150 DISP  "LATITUDE =";
160 INPUT L
170 PRINT "LATITUDE="L
180 DISP  "DATE=";
190 INPUT  D1
200 PRINT  "DATE="D1
210 DISP  "DECLINATION=";
220 INPUT  D
230 PRINT  "DECLINATION="D
240 DISP  "EQUATION OF TIME=";
250 INPUT  E
260 PRINT  "EQUATION OF TIME ="E
270 DISP  "IF STANDARD TIME; ENTER 1";
280 INPUT  C
290 IF C=1  THEN 310
300 GOTO 330
310 PRINT "STANDARD TIME IS INPUT"
320 GOTO 340
330 PRINT "DAYLIGHT SAVINGS TIME IS INPUT"
340 PRINT
350 WRITE (15,510)
360 WRITE (15,520)
370 DISP "TIME=HOURS,MINUTES";
380 INPUT H, M
390 M1=M/60
400 T=H+M1
410 IF C=1 THEN 430
420 T=T-1
430 N=12,083+E
440 H1+ABS((T-N)*15)
450 DEG
460 Z=SINL*SIND+COSL*COSD*COSH1
470 A=ATN(SQR(1-Z↑2)/Z)
480 WRITE (15,500)D1,H,M,A
490 GOTO 370
500 FORMAT F7,0,3X,F3.0,":",F3.0,5X,F6.2
```

```
510 FORMAT 2X, "DATE",6X,"LOCAL",5X,"ZENITH"
520 FORMAT "            TIME     SUN ANGLE"
530 END
```